

AD-A037 246

UNITED TECHNOLOGIES RESEARCH CENTER EAST HARTFORD CONN F/G 11/6
DEVELOPMENT OF DIRECTIONALLY SOLIDIFIED EUTECTIC NICKEL ALLOYS --ETC(U)
NOV 76 F D LEMKEY N62269-76-C-0107

UNCLASSIFIED

UTRC/R76-91251A-3

NADC-7520A-30

NL

1 OF 1
AD
A037246



END

DATE
FILMED
4-77

76-912518-3

NADC 75208-30

B.S.

ADA 037246

Development of Directionally Solidified Eutectic Nickel Alloys for Use in Aircraft Gas Turbines at Metal Temperatures Exceeding 1000°C

Final Report

Prepared under Contract N62269-76-C-0107

Naval Air Development Center
Warminster, Pennsylvania 18974

for

Naval Air Systems Command
Department of the Navy
Washington, DC 20361

by

F.D. Lemkey

November 1976

DDC
RECEIVED
MAR 18 1977
A

**UNITED TECHNOLOGIES
RESEARCH CENTER**



**UNITED
TECHNOLOGIES™**

EAST HARTFORD, CONNECTICUT 06108

" APPROVED FOR PUBLIC RELEASE—DISTRIBUTION UNLIMITED"

20. Cont'd

of alloying. Tantalum and rhenium additions improved the high temperature creep strength and tantalum additions combined with chromium (i.e. Ni-32 w/o Mo-5.5 w/o Al-3 w/o Cr-1 w/o Ta) yielded an alloy whose cyclic oxidation resistance at 1000°C compared favorably to the outstanding oxidation resistant nickel-base superalloy, B-1900. Since the measured coefficient of thermal expansion of $\gamma'/\gamma-\alpha$ alloys are below the CTE's of conventional coatings the requirement of a compatible lower expansion coating was indicated.

The ultimate shear strengths of $\gamma'/\gamma-\alpha$ alloys at intermediate temperatures (760-880°C) were found to be equivalent to nickel base superalloys. However, the shear creep rupture properties at 760°C were below those of the more isotropic superalloys. The thermal fatigue resistance of $\gamma'/\gamma-\alpha$ alloys was found to be dependent on aluminum content. Alloys containing 7.8 w/o Al exhibited substantially greater resistance to cyclic thermal fatigue (400-1122°C) under stress than both D.S. Mar M200 + Hf and $\gamma/\gamma'-\delta$.

gamma/gamma'-delta.

** gamma'/gamma-alpha*

ACCESSION No.	
NTIS	✓
DOC	✓
CLASSIFIED	
JUSTIFICATION	
BY	
DISTRIBUTION STATEMENT	
DIS. STATEMENT	
A	

**UNITED TECHNOLOGIES
RESEARCH CENTER**



East Hartford, Connecticut 06108

Report R76-912518-3

Development of Directionally Solidified Eutectic
Nickel Alloys for Use in Aircraft Gas
Turbines at Metal Temperatures
Exceeding 1000°C

Final Report
Contract N62269-76-C-0107

Period: April 8, 1976 to October 7, 1976

REPORTED BY

F. D. Lemkey, Principal Scientist
High Temperature Materials

APPROVED BY

E. R. Thompson, Manager
Materials Sciences

Development of Directionally Solidified Eutectic Nickel
Alloys for Use in Aircraft Gas Turbines at Metal
Temperatures Exceeding 1000°C

TABLE OF CONTENTS

I.	INTRODUCTION	1
II.	EXPERIMENTAL PROCEDURES	3
	2.1 Melting and Solidification	3
	2.2 Differential Thermal Analysis	3
	2.3 Mechanical Testing	4
	2.3.1 Stress Rupture	4
	2.3.2 Shear	4
	2.3.3 Thermal Cycling	4
	2.4 Thermal Expansion Measurements	5
	2.5 Oxidation and Sulfidation Testing	5
III.	RESULTS AND DISCUSSION	6
	3.1 Alloying and Solidification	6
	3.2 Mechanical Properties	9
	3.2.1 Longitudinal Stress Rupture	9
	3.2.2 Transverse Stress Rupture	10
	3.2.3 Tensile Shear Properties	10
	3.2.4 Creep Shear Properties	11
	3.2.5 Thermal Cycling	11
	3.3 Long Term Isothermal Exposure Tests	12
	3.4 Thermal Expansion Measurements	12
	3.5 Oxidation and Sulfidation Tests	13
IV.	CONCLUSIONS	15
	REFERENCES	16
	TABLES I - XV	18
	FIGURES 1 - 22	

I. INTRODUCTION

The requirement for advanced turbine alloys possessing high metal temperature ($>1000^{\circ}\text{C}$) capability from the standpoint of creep strength, melting point, fabricability, and corrosion resistance continues to be a critical pacing factor in the development of higher performance gas turbine engines. Today's directionally solidified eutectic superalloys offer the potential for significant increases in turbine blade temperature capability (i.e. $100\text{--}150^{\circ}\text{F}$). This can be compared with the steady improvement rate of perhaps $15^{\circ}\text{F}/\text{yr}$ for conventional superalloys over the past thirty years. The ability to perform at more elevated temperatures is achieved through design of multicomponent eutectic alloys where one or more phases serve as the matrix and the other aligned phase performs as the reinforcement. In addition to achieving high strength, these *in situ* composite materials exhibit excellent long term microstructural stability at temperatures exceeding 0.9 of their absolute temperature. The successful utilization of the cast precipitation hardenable nickel-base superalloys, such as Mar M200, has demonstrated that the notoriously poor thermal fatigue resistance of this class of superalloys can be overcome by directional solidification. These benefits, derived from aligned grain boundaries and preferred orientations, have also been obtainable in the design of certain eutectic superalloys and oxide dispersion and perhaps refractory wire strengthened superalloys of even greater temperature capability (Refs. 1-6).

The two eutectic superalloys (i.e. $\gamma/\gamma'\text{-}\delta$ (Ref. 3) and NiTaC-13 (Ref. 4)) under current development in the United States for engine hardware both consist of strong ductile face centered cubic gamma matrix containing gamma prime, Ni_3Al , precipitates reinforced by aligned more brittle phases. Although possessing excellent stress rupture strength, these eutectic superalloys exhibit reduced total elongations due in part to the plastic constraint of the matrix by the less ductile reinforcing phase. To improve the longitudinal and off-axis ductility, the design of a ductile-ductile eutectic superalloy was initiated under Contract N62269-75-C-0129 (Ref. 2). Stress rupture properties of certain $\gamma'/\gamma\text{-}\alpha$ alloys, parallel to the direction of growth, indicated a greater than 100°F improvement over D.S. Mar M200 + Hf and improved ductility at intermediate (760°C , 1400°F) as well as elevated (1093°C , 2000°F) temperatures.

The monovariant eutectic $\gamma'/\gamma\text{-}\alpha$ path investigated under the past contract was derived from the quasibinary $\gamma'\text{-}\alpha$ ($\text{Ni}_3\text{Al}\text{-}\text{Mo}$) system. This monovariant eutectic is composed of the nickel solid solution γ and the ordered compound Ni_3Al , γ' in varying amounts depending on the aluminum content and allows rather extensive alloying by ternary, quaternary and even quinary additions, provided solubility in both γ , γ' and α phases is permitted. The objective of this program

was to optimize by compositional and process variations certain key mechanical and physical properties of the γ'/γ - α system including stress rupture, shear, and transverse strength and oxidation/sulfidation resistance. The density, melting range, thermal expansion coefficients (parallel, perpendicular and 45° to phase alignment) and low cycle thermal fatigue characteristics of the system were also examined. The overall objective of the program however was to obtain an isotropically ductile eutectic alloy superior to those directionally solidified eutectic alloys under current consideration for use in aircraft gas turbines at metal temperatures exceeding 1000°C .

II. EXPERIMENTAL PROCEDURES

2.1 Melting and Solidification

Master melts of the various alloys investigated were made in new recrystallized alumina crucibles in a Heraeus vacuum induction melting furnace powered by a 30 kW motor generator and pumped by a 25 cm (10 in.) vacuum system. The system was exhausted to approximately 0.001 N/m^2 (10^{-5} torr) and then back filled with high purity argon to provide a dynamic 200 liters per hr (~ 7 cfh) inert cover at atmospheric pressure. Power to the furnace coil was slowly increased until melting of the nickel, chromium and molybdenum charge material was achieved. Aluminum was then added separately to the melt. Subsequently the melt was held at a constant temperature of $\sim 1400^\circ\text{C}$ (2550°F) for a 15-20 min homogenization period prior to pouring into copper chill molds. The purity of the starting materials used is presented in Table I. Impurities detected by atomic absorption analysis are noted therein.

Each resulting cast alloy bar was usually directionally solidified vertically within a nominally 0.95 cm ($3/8$ in.) diameter 99.7% recrystallized alumina cylindrical crucible whose wall thickness was nominally 2 mm. Vertical controlled solidification was accomplished in a high gradient apparatus described in Ref. 1. In this setup a known mass of alloy typically 200 gms, contained in a both ends open or one end closed cylindrical alumina crucible, is positioned within the induction coil, water spray ring, and constant water level tank. With the impinging water spray turned on, melting is accomplished by inductive coupling with the stationary graphite sleeve. Power requirements are established from empirical trials or experiments instrumented with thermocouples. The freezing is controlled by the withdrawal of the Al_2O_3 crucible through the water spray ring. In this setup thermal gradients in the liquid of approximately $300\text{-}400^\circ\text{C/cm}$ were routinely achieved. Excluding small end affected regions the rate of freezing is found to be equal to the velocity of crucible withdrawal over the entire specimen length solidified. Each directionally solidified bar was given a laboratory number and each subdivided specimen was identified by a dash (-01, -02, etc.) and numbered from the end first solidified.

2.2 Differential Thermal Analysis

Small slugs were machined from directionally solidified alloys and inserted in special alumina crucibles. A differential thermal analysis measurement of the melting and freezing behavior of certain ternary and modified Ni-Al-Mo alloys were made relative to pure nickel using a differential thermal analysis apparatus described elsewhere (Ref. 7). The platinum vs platinum-10% rhodium thermocouple used was calibrated against a pure silver standard and the accuracy of the

temperature was within $\pm 2^{\circ}\text{C}$. The liquidus temperature was normally determined during cooling and the solidus during heating from the respective exothermic and endothermic inflections of the temperature-differential temperature traces.

2.3 Mechanical Testing

2.3.1 Stress Rupture

Stress rupture tests on samples machined parallel to and perpendicular to the solidification direction were performed between $1400\text{--}2039^{\circ}\text{F}$ ($760\text{--}1115^{\circ}\text{C}$) in air. Tests were performed in accordance with ASTM specification E139-6, with specimens of gage diameter 0.110 in. (0.28 cm) and nominal gage length 0.50 in. (1.27 cm) with 5/16-18 threaded ends. Crosshead extension was measured during certain tests and elongation and reduction of area measurement were made from mating the fractured halves under a 5X magnifier and using calipers.

2.3.2 Shear

Longitudinal tensile shear and creep shear specimens were machined to the double bolt head specimen illustrated in Fig. 1 for measurement of the shear strength parallel to the growth direction and α fiber phase alignment. The specimens consisted of a 1/4 in. (0.64 cm) diameter bolt shank with two 1/8 in. (0.32 cm) thick heads which were attached to a fixture shown in Fig. 2. The fixture consisted of two high temperature slotted button head adapters and split ring washers to insure full bearing on the specimen heads. Longitudinal shear tests were conducted in air between $1400\text{--}1600^{\circ}\text{F}$ ($760\text{--}870^{\circ}\text{C}$) at a loading rate of 0.01 in./min (0.025 cm/min) using a four screw machine. Shear creep tests were performed on the same specimen geometry in air at 1400°F (760°C) only.

2.3.3 Thermal Cycling

The apparatus used for thermal cyclic exposure is presented in Fig. 3, and consists of a control circuit and specimen holding and loading fixture. Samples were heated by self resistance and were loaded by means of weights pulling on a cable attached to a load transfer wheel having a diameter ratio of six to one. The control circuit adjusted input voltage automatically so that temperature, which was measured by a welded-on thermocouple, was cycled between the set limits. Temperature limits used were 750°F (400°C) to 2050°F (1122°C) except for one set of specimens where the upper limit was 1900°F (1038°C). The applied stresses for the samples varied between 5-15,000 psi.

The temperature distribution produced by this apparatus has been shown (Ref. 8) to be roughly parabolic along the specimen length, and to vary by less than 10°F through the bar at the center while that point is held at 2050°F . One-half of the specimen holder travels freely on linear ball bushings so that

resistance to thermal expansion and contraction due to the weight of the carriage, lines and friction produced an axial stress of only about 25 psi on the specimen. The temperature cycle used in this investigation was of approximately 2 min duration and produced maximum heating and cooling rates of about 45°F/sec. A flowing argon atmosphere (focused as a jet at the center of the specimen) was used to protect the specimen and thermocouple from severe oxidation (although a surface layer of oxide did form on all specimens and to rapidly cool the specimen from the maximum temperature).

Specimen expansion and contraction was monitored using an LVDT attached to the specimen support and traveling stages. A trace of the specimen length change with each cycle and over the period of the test was therefore obtained. An example of one such trace is presented in Fig. 4. Traces such as this could be used for correlating microstructural data from interrupted tests with the extent of deformation or fraction of thermal cyclic life.

2.4 Thermal Expansion Measurements

Dilatation curves were generated using a Theta DilatronicTM II dilatometer. A single push rod setup was used with a reference material of Al₂O₃. The specimen was heated at a rate of 20°F/min to 2150°F (1180°C) and cooled at a slightly faster cooling rate. From measurements of the difference in expansion between the sample and an accurately known standard reference material, high accuracy (+30 ppm) expansion measurements were obtained.

2.5 Oxidation and Sulfidation Testing

Rectangular specimens were ground and lapped through 600 grit SiC paper and cleaned with trichloroethylene from modified and base line ternary $\gamma'/\gamma-\alpha$ D.S. alloys so as to yield samples with their longer rectangular surfaces parallel and perpendicular to the direction of eutectic growth. Cyclic oxidation was evaluated at 1290°F (700°C) and 1830°F (1000°C). In these tests each cycle consisted of exposing the sample for 2 hrs to elevated temperature, cooling to room temperature, lightly brushing the sample to remove the nonadherent scale and weighing. This procedure was repeated for a total of fifteen (15) cycles.

Hot corrosion tests were performed at 1650°F (900°C) in air. This testing involved coating the ground and lapped sample with 0.5 mg cm⁻² Na₂SO₄ and cycling (50 min in the furnace followed by an air cool) for comparison with previous test results reported in Ref. 2.

III. RESULTS AND DISCUSSION

3.1 Alloying and Solidification

To meet this program's objective of providing an isotropically ductile eutectic alloy superior to those directionally solidified eutectic alloys ($\gamma/\gamma'-\delta$, NiTaC-13, and COTAC 74) under current consideration, alloys based on the pseudobinary isopleth $\gamma'-\alpha$ (Ni₃Al-Mo, Ref. 2) were selected for further compositional and mechanical property characterization and optimization. It was previously postulated that a monovariant trough extended from the $\gamma' + \alpha$ pseudobinary eutectic with decreasing aluminum content (Refs. 2,9). Numerous ternary and higher order multivariant compositions that solidify in a coupled manner and result in microduplex composite structures were thus predicted. More than twenty compositions were examined, including those in Table II, to locate the monovariant trough where $L \xrightarrow{\Delta T} \gamma'/\gamma + \alpha$, where γ'/γ refers to the presence of more γ' than γ after solidification. The locus of the monovariant trough was determined from the absence of γ , γ' or α dendritic phases in directionally solidified specimens polished longitudinally to reveal primary phase compositional segregation during directional freezing. The location of a ternary reaction point or a maximum melting composition on the monovariant eutectic trough was found near the composition Ni-31.5 w/o Mo-6.2 w/o Al ($\rho \sim 8.46$ gm/cc) from DTA measurements as shown in Table III. The slopes of the liquidus temperatures over the compositional range of interest, i.e. 3.7-9.8 w/o Al were shallow thus preventing a more precise determination of the class of these reactions. Examination by replication and subsequent transmission electron microscopy of quenched interfaces revealed the presence of fine γ' at the L/S interface for the Ni-31.5 w/o Mo-6.2 w/o Al alloy. This fine gamma prime was observed to coarsen and agglomerate around the α -molybdenum fibers as one examined the aligned structure further away from the quenched L/S interface. In another study (Ref. 10) heat treated and quenched samples near this composition were interpreted as evidence for the reaction $L \rightarrow \gamma + \alpha$ with subsequent rejection of aluminum atoms from the α Mo phase to promote segregation of γ' to the fiber interfaces. No doubt the large retrograde solubility of γ' in γ nickel causes considerable difficulty in the interpretation of these experiments. For example, no DTA signal was detected for the γ' solvus in the Ni-Al-Mo alloys examined (Table III) contrary to that found in common nickel base superalloys. A quaternary alloy containing 3 w/o chromium (Ni-29.5 w/o Mo-6.2 w/o Al-3 w/o Cr) indicated no liquidus and solidus temperature separation as shown in Fig. 5 and was interpreted as being either close to a quasibinary or ternary eutectic reaction.

Chromium substitutions for molybdenum in the nominal composition Ni-31.5 w/o Mo-6.2 w/o Al and Ni-35 w/o Mo-5.5 w/o Al were examined at one weight percentage intervals to 6 w/o chromium (for the former to 9 w/o chromium) as described in Table IV. For each of these levels of chromium plane front growth

conditions were observed at an equivalent G/R processing ratio of $\sim 100^\circ\text{C hr cm}^{-2}$. Chromium was expected to partition to both the γ and α phases as it is extensively soluble and completely miscible in the γ and α phases respectively and relatively insoluble in γ' . To examine this point, chemical separation of α -Mo from γ'/γ - α alloys was accomplished by dissolving the γ'/γ matrix in hot HCl activated by hydrogen peroxide (Ref. 11) and removing the floating rods from the surface followed by a water rinse and subsequent drying cycle. Wet chemical analyses of the extracted α -Mo rods are presented in Table V and Fig. 6. It can be inferred from the correlation of chromium content in α -Mo, where complete solid state miscibility exists, to the chromium content in the nominal alloy that chromium atoms also partition to the γ phase. As will be discussed later, this partitioning of chromium promotes a desirable oxidation resistant γ phase within the matrix.

The transition metals, cobalt and iron, were substituted on an atom basis for nickel at intervals to 9 and 5 w/o respectively to examine their effects on the γ' solvus temperature. Plane front growth conditions could be achieved for 5 w/o Fe and 7 w/o Co under the described growth conditions of Table IV. Electron photomicrographs of replicated transverse sections are shown in Fig. 7 for example substitutions.

Titanium and tantalum were substituted because of their extensive solubility in all three phases, γ , γ' and α and to determine their solid solution hardening effects in γ/γ' . Titanium additions at 1.5 w/o caused the L/S interface to degenerate to cells under a gradient of $\sim 300^\circ\text{C/cm}$ and a growth velocity of 3 cm/hr. Additional amounts of Ti in conjunction with 3 w/o Cr indicated that a new phase derived from the melt was present. The presence of over four weight percent Ta destroyed the faceted nature of the α , Mo phase interfaces as shown in Fig. 8 and cellular coupled growth was observed to 7 w/o Ta under the previously stated growth conditions for Ti modified alloys. Carbon additions to the Ta and Ti bearing alloys did not result in the expected carbide precipitation with the α Mo phase but instead resulted in interesting four phase alloys wherein the γ/γ' matrix contained aligned α , Mo platelets and rods together with another aligned as yet unidentified harder fibrous phase as shown in Fig. 9 and identified as phase X. Electron diffraction studies of A76-272 (Ni-32Mo-5.5Al-1Ta-3Cr-0.066C) (Fig. 10) indicated that the orientation of the γ/γ' and α phases remained constant from grain to grain as described previously (Ref. 2), while the lattice parameter of the unknown phase, X, was very large, $\sim 8.2\text{\AA}$, and could not be indexed with known MC, M_6C phases.

Re and W were added as indicated in Table III since they have been shown to be potent solid solution and grain boundary strengtheners at relatively low concentrations. Both elements were soluble to at least 3 w/o in the γ'/γ - α system but required reduced freezing velocity to produce aligned microduplex structures.

The effect of selected modifications on the interfiber spacing of the basic ternary Ni-35 w/o Mo-5.5 w/o Al was studied as it appeared that certain elements might provide a means of reducing α -fiber size and spacing without changing the solidification velocity. Seven compositions including Ta, W, and Cr modifications were examined for variation in λ ; determined by counting the number of rods in an area A and calculating their average interfiber spacing from the relationship $\bar{\lambda} = \sqrt{A/N}$ where N is the number of rods in area, A. The results are shown in Table VI and indicate a trend for more widely spaced α fibers of slightly larger size by additions of W and Ta atoms.

Several microstructural features were examined in greater detail, one being the improvement of microstructural perfection (uniformity of size and spacing) which is a subject of a parallel investigation (Ref. 12). An interesting phenomena which is present in grain boundaries of almost all directionally solidified γ'/γ - α alloys is the presence of the lamellar form of α Mo. This transition in morphology is believed associated with a local liquid solid interface curvature change (cusp) but must be distinguished from a much finer and more wave-like perturbation which manifests itself in microcellular structures within eutectic grains as shown in Fig. 8 and which can be controlled (eliminated) by increasing the thermal gradient in the melt during solidification or by decreasing the solidification velocity. The grain boundary region which exhibited this rod to lamellar transition was examined using an electron microbeam probe for additional evidence of impurities and/or chemical composition gradients derived from nonisothermal solidification conditions. Two samples representing varying directional solidification conditions and melt casting (raw materials) practices were examined as identified below:

UTRC A76-716-01 Ni-31.5 w/o Mo - 6.2 Al (nominal), G \sim 300°C/cm, R = 3 cm/hr
Inter g.b. Ni-33.4 \pm .7 Mo - 5.8 \pm .1 Al; Intra g.b. Ni-32.2 \pm .5 Mo - 6.0 \pm .1 Al

PWA E591-9 Ni-31.5 w/o Mo - 6.2 Al (nominal), G \sim 120°C/cm, R = 2 cm/hr
Inter g.b. Ni-31.3 \pm .8 Mo - 5.8 \pm .1 Al; Intra g.b. Ni-32.1 \pm .5 Mo - 5.6 \pm .6 Al

The mean chemical composition was determined from a minimum of five line traces of inter and intragrain regions. No meaningful composition gradient could be detected from these results and no impurities, whose atomic number was greater than sodium, were detected above 0.25 w/o. Thus, no conclusion regarding the origin of α -Mo size and spacing change at γ'/γ - α eutectic grain boundaries could be reached based on segregation.

3.2 Mechanical Properties

3.2.1 Longitudinal Stress Rupture

The rupture strengths of various monovariant eutectic alloys tested in air are presented in Table VII. The optimum aluminum content can be inferred from the plot of Fig. 11 to vary between 4-8 w/o for maximum rupture life at 1900°F and 30 ksi. Two data points had to be extrapolated from the Larson-Miller parameter-stress plot for 7.0 and 7.8 w/o Al alloys (Ref. 2) to complete the range. The deleterious effect cellular microstructure has on the high temperature stress rupture lives of this class of alloy is noted for alloys directionally solidified at 10 cm/hr. For comparison purposes the rupture life for D.S. Mar M200 + Hf at these conditions of stress and temperature would be between 10-15 hrs.

The effect of chromium on the rupture life at 1900°F and 30 ksi was studied most extensively at an aluminum level of 5.5 w/o compared with the previous study of chromium content variation at 6.2 w/o aluminum (Ref. 2). Once again there was significant scatter in the rupture lives of the 3 w/o Cr specimens in particular as shown in Fig. 12. On examination of the fracture surface of each specimen it was determined that cellular and dendritic α structural defects existed within the gage section of two of the four specimens containing 3 w/o Cr which exhibited rupture lives below 100 hrs. It appears that specimens which contain totally microduplex eutectic structures possessing microcells or bimodal α rod distributions within grains but no macrocells (wherein rods or platelets bend deeply in the radial direction of heat flow) exhibit slight, if any, statistical reduction in strength due to the presence of 3 w/o chromium.

The previous marked dependence of rupture life on chromium content at an aluminum level of 6.2 w/o (Ref. 2) was examined metallographically. Although some of the scatter in data could be attributed to the presence of α dendrites, cellular bands and other solidification defects existing within the gage volume, a marked degree of accelerated coarsening of the α rods was observed both in the stressed and unstressed regions of the rupture specimen. A montage depicting this breakup of the highly faceted α , Mo interfaces is shown in Fig. 13. To ascertain a driving force (i.e. reduction of interfacial energy mechanism) for this marked change in microstructural stability with chromium content, the chemical composition change in α -Mo and its effect on the diffusional stability was sought. The rate of coarsening ("Ostwald ripening") is expected to be determined by either bulk (volume) diffusion or by an interface-controlled reaction (Refs. 13,14). Chromium appears to be a fast moving diffusional species compared with the larger substitutional atoms W, Ta or Re. Thus, some of this accelerated diffusion and subsequent coarsening may be retarded by combined additions with W, Ta or Re for example. Experimental confirmation of this prediction is observed in the stress rupture life results of the Ta and W modification series with 3 w/o Cr.

The effect of cobalt and iron additions were in general deleterious to the rupture life of the base line Ni-35Mo-5.5Al ternary alloy as shown for cobalt in Fig. 14. On the other hand, tantalum to 2 w/o and 1 w/o rhenium additions exhibited improvements in the rupture life compared with the base line ternary alloy at the 1 w/o levels as indicated in Fig. 15. This behavior with some degree of hindsight would be expected as certain atoms are more mobile than others at creep temperatures. Tungsten, tantalum and rhenium atoms are less mobile than iron and cobalt atoms at temperatures in the neighborhood of 1900°F. Hence the former atoms form effective deterrents to grain boundary creep. Thus to be effective as a solution hardener and grain boundary strengthener for the γ/γ' - α alloys the alloying element should be less mobile at the creep temperature than are the atoms of the matrix.

In general with all the modifications as well as the base ternary mono-variant eutectic alloys, faster processing (i.e. R ~10 cm/hr vs 3 cm/hr) resulted in inferior rupture lives in both 1400 and 1900°F tests, indicating again the desirability for aligned planar front growth for optimum creep resistance.

3.2.2 Transverse Stress Rupture

A fully aligned slab casting (3 in. x 6 in. x 3/8 in.) of Ni-31.5 w/o Mo-6.2 w/o Al was prepared by PWA's Manchester Experimental Foundry at a growth rate of 3 cm/hr under an estimated gradient of 100°C/cm. Specimens transverse to the growth direction were machined for stress rupture testing. The results of these tests are presented in Table VIII. There appears to be a small ductility decrease in transverse stress rupture specimens tested at 1900 and 2000°F. The transverse rupture strength and ductility is greater than that observed for the γ/γ' - δ (Ref. 3) especially at the intermediate temperatures. A Larson-Miller parameter plot was constructed for the data of Table VIII and is presented in Fig. 16.

Metallographic examination of fracture surfaces in the SEM indicated grain boundary related fracture paths at 1400°F as shown in Fig. 17 and grain boundary sliding at 2000°F. As was previously observed, the mean free path of matrix γ/γ' is greatest where the lamellar morphology of α , Mo intersects at grain boundaries suggesting this region as a preferential deformation site.

3.2.3 Tensile Shear Properties

Tensile shear test results on ternary modifications of γ/γ' - α and quaternary additions of chromium are presented in Table IX and Fig. 18 for bolt head test methods. These results represent minimum values of shear as both bolt ends were machined to equivalent dimensions and were loaded equally. Examination of the broken test specimens indicate a large component of grain boundary shear at both

test temperatures. These results show significant improvements of shear strength, particularly for the chromium modified composition of $\gamma/\gamma'-\alpha$ at 760°C (1400°F) compared with the current first generation eutectic $\gamma/\gamma'-\delta$. This result is of particular importance because a 3D stress analysis of a eutectic blade root recently completed by PWA indicated shear stresses in advanced attachments selected for eutectic blade evaluation exceed the ultimate shear strength of the $\gamma/\gamma'-\delta$ system. Comparison of the $\gamma/\gamma'-\alpha$ results with B-1900 data indicate that shear properties for this ductile-ductile system can meet typical superalloy shear properties. Further improvements are expected by heat treatment of the γ/γ' matrix as was observed for the $\gamma/\gamma'-\delta$ and superalloys.

3.2.4 Creep Shear Properties

Results of ultimate shear strength tests on $\gamma'/\gamma-\alpha$ alloys in the previous section indicated the strength in pure tensile shear for longitudinally aligned specimens approached and, for certain alloy modifications, exceeded those of cast nickel-base superalloys (i.e. B-1900) at intermediate temperatures (1400-1600°F). Testing in creep rupture was begun to further characterize this mechanical property critical to the design of "fir tree" turbine blade root. Preliminary results of these tests together with base line data derived from other programs (Ref. 3) are presented in Table X. In comparison with the tensile shear properties, the shear creep strength values of both eutectics were considerably below those for nickel-base superalloys.

3.2.5 Thermal Cycling

The ability of the monovariant eutectic alloys to withstand repeated cycling from 750°F-2050°F (400-1122°C) under load was measured. A stress level of 10,000 psi was selected as representative of that experienced in an engine. The samples were tested in two ways; one condition was to simply cycle the specimen under no load to evaluate the role of internal stresses and the other condition was under an external load. One problem which may arise when an aligned two phase material is applied in a cyclic thermal environment is that internal damage may occur as a result of the different coefficients of thermal expansion between the phases. This problem is different from the thermal fatigue that arises in materials as a result of restrained expansion and contraction of these sections.

The results of unloaded thermal cycling of $\gamma'/\gamma-\alpha$ alloys are summarized in Table XI. Unexpectedly a dimensional instability was observed for monovariant alloys containing 5.5 and 6.2 w/o Al.

The 7.8 w/o Al specimen on the other hand was dimensionally stable and microstructurally closely resembled a previous test on Ni-27.0 w/o Mo-8.0 w/o Al where after 3000 cycles the 2000°F hot tensile strength was measured at a very slow strain rate ($\dot{\epsilon} \approx .001$) and revealed no change in strength or ductility. Although samples of $\gamma/\gamma'-\delta$ and Mar M200 were not cycled unloaded, prior experience with these materials indicates that no dimensional instabilities are to be expected.

The results of loaded (varying stress) thermal fatigue testing is also summarized. All samples were tested until failure or 3000 Ω was reached, with the number of cycles to failure used as a stability criterion, and reduction of area as a measure of ductility. Again the dependence of thermal fatigue life on aluminum content was exhibited with the alloy containing 7.8 w/o Al indicating considerably greater thermal fatigue resistance than directionally solidified Mar M200 + Hf and the first generation eutectic superalloy $\gamma/\gamma'-\delta$. A plot of the extension, measured continuously by LVDT, versus number of cycles is presented in Fig. 19. The cause of the abruptness in the generation of a smooth three stage creep curve especially in the transition region from steady state to third stage creep is not understood. It was present in all the tests which went over 500 cycles and could not be correlated with random power fluctuations. It may have its origin in internal dimensional changes (i.e. void generation) which raises the local resistance and temperature before the controlling surface thermocouple reacts to cause a power reduction.

3.3 Long Term Isothermal Exposure Tests

Three ternary $\gamma'/\gamma-\alpha$ alloys containing 7.8, 5.5 and 4.7 w/o Al were exposed for 1000 hrs at 1100°C to determine the thermal stability of the microstructure. No change was observed in the facets which make up the phase interfaces between γ' and α . Some solutioning and subsequent precipitation of the γ' was observed to take place within the γ phase. A microstructural account of this exposure is presented in Fig. 20. The square shaped interfaces indicated a strong interphase crystallographic relationship previously determined (Ref. 9) to be:

Growth Direction		[001] γ'		[001] γ		[001] α
Interfaces		(100) γ'		(100) γ		($\bar{1}$ 10) α
		(010) γ'		(010) γ		($\bar{1}$ 10) α

3.4 Thermal Expansion Measurements

Dilatation curves showing alloy expansion as a function of temperature for $\gamma'/\gamma-\alpha$ (Ni-31.5 w/o Mo-6.2 w/o Al) in different orientations are presented in Fig. 21. The curve was generated by Dr. F. Douglas of UTRC using a Theta Dilatronic II dilatometer. The coefficient of thermal expansions were calculated

for every 100°C temperature interval from the average slope of the data curve and are presented in Table XII. The CTE is below all phases of the MCrAlY coating system except α Cr (Ref. 15) and is due to the large volume fraction of α , Mo in the alloy. This indicates the requirement to develop a lower expansion protective coating for $\gamma'/\gamma-\alpha$ eutectic alloys.

3.5 Oxidation and Sulfidation Tests

Rectangular specimens were ground from modified and base line $\gamma'/\gamma-\alpha$ so as to yield samples with their longer rectangular surfaces parallel or perpendicular to the direction of eutectic growth. Two $\gamma'/\gamma-\alpha$ compositions were examined in both orientations to determine any anisotropy effects of surface stability. The cyclic oxidation characteristics were evaluated at 700°C (1290°F) and 1000°C (1830°F) under the direction of Dr. J. Smeggil. In these tests each cycle consisted of exposing the sample for 2 hrs to elevated temperature, cooling to room temperature, lightly brushing the sample to remove the nonadherent scale and weighing. This procedure was repeated for a total of fifteen (15) cycles. The data for the cyclic oxidation tests at 700 and 1000°C are presented in Tables XIII and XIV. At 700°C the data suggest no major amounts of oxidation. However, at 1000°C the data indicate that the overall oxidation resistance of the base composition Ni-31.5 w/o Mo-6.2 w/o Al is markedly improved by additions of Cr and perhaps Ta. To a first order approximation the oxidation behavior of the Cr containing alloys as seen in Fig. 22 is comparable to that of B-1900. The extent of oxidation on sections parallel to, and transverse to, the α -Mo fibers appeared to be similar.

The retained scales of the oxidized samples were examined with Cu K_{α} , X radiation. Positive identification of the phases for samples oxidized at 700°C was difficult due to the presence of only weak lines in the patterns. The preliminary fit of the results is indicated below for several $\gamma'/\gamma-\alpha$ alloys:

A76-200-L	Ni-31.0 w/o Mo-6.2 w/o Al-3.0 w/o Cr	NiO, Mo ₉ O ₂₆
A76-200-T	Ni-31.0 w/o Mo-6.2 w/o Al-3.0 w/o Cr	NiO, Mo ₉ O ₂₆
A76-289-03	Ni-37.5 w/o Mo-4.0 w/o Al	NiO, MoO ₂
A76-299-04	Ni-32.0 w/o Mo-5.5 w/o Al-1.0 w/o W	NiO, Mo ₉ O ₂₆
A76-267-03	Ni-32.0 w/o Mo-5.5 w/o Al-1.0 w/o Ta-3.0 w/o Cr	NiO, Mo ₉ O ₂₆

For the scales of samples oxidized at 1000°C, the following "best fit" candidate oxide phases were identified:

E-591-T	Ni-31.5 w/o Mo-6.2 w/o Al	NiMoO ₄ , NiAl ₂ O ₄
A76-200-L	Ni-31.0 w/o Mo-6.2 w/o Al-3.0 w/o Cr	NiMoO ₄ , NiAl ₂ O ₄
A76-289-03	Ni-37.5 w/o Mo-4.0 w/o Al	NiMoO ₄ , NiAl ₂ O ₄
A76-299-04	Ni-32 w/o Mo-5.5 w/o Al-1.0 w/o W	NiMoO ₄ , NiAl ₂ O ₄
A76-267-03	Ni-32 w/o Mo-5.5 w/o Al-1.0 w/o Ta-3.0 w/o Cr	beginnings of both NiMoO ₄ & NiAl ₂ O ₄ just above background

Additionally, a hot corrosion test was performed at 900°C (1650°F) in air. This test involved coating the sample with 0.5 mg/cm² Na₂SO₄. Then the samples were cycled (50 min in the furnace followed by an air cool) twice for comparison with prior results reported by E. J. Felten (Ref. 2). The mass gains for the samples after hot corrosion cyclic testing are presented in Table XV. It is clear that the modified alloys are only slightly less sensitive to hot corrosion. Continued exposure to Na₂SO₄ leads to continued rapid attack and oxide scale spalling.

IV. CONCLUSIONS

1. The oxidation behavior of chromium (and tantalum) containing $\gamma'/\gamma-\alpha$ (i.e. Ni-32 w/o Mo-5.5 w/o Al-3 w/o Cr-1 w/o Ta) was found to compare favorably to that of an outstandingly oxidation resistant nickel base superalloy, B-1900, at 1000°C. Moreover, the extent of oxidation penetration on sections parallel and transverse to the α -Mo fibers was similar. Chromium was found to segregate to both the α -Mo fibers and the γ matrix phase where it is completely miscible and extensively soluble, respectively.

2. Extensive (>7 w/o) substitutions of chromium, cobalt, iron, and tantalum and more limited substitutions of tungsten, rhenium, titanium, and carbon demonstrated the wide flexibility of alloying within the monovariant system, $\gamma'/\gamma-\alpha$. An interesting in situ composite consisting of two aligned fibrous phases α -Mo and an unidentified but harder X phase within a γ'/γ matrix was found for the tantalum and carbon modified alloy, Ni-32 w/o Mo-5.5 w/o Al-3 w/o Cr-1 w/o Ta-0.066 w/o C.

3. Tantalum, tungsten and rhenium modifications exhibited improved $\gamma'/\gamma-\alpha$ creep rupture strength. Additions of these higher melting elements proved to be more effective than additions of cobalt, iron, titanium or chromium in providing matrix hardening and microstructural thermal stability.

4. The ultimate tensile shear strengths of $\gamma'/\gamma-\alpha$ alloys at intermediate temperatures 760-876°C (1400-1600°F) were found to be equivalent to nickel base superalloys. However, the shear creep rupture lives at 760°C (1400°F) were below superalloys. Further shear property optimization was predicted from heat treatment and/or thermomechanical processing.

5. Thermal fatigue resistance of $\gamma'/\gamma-\alpha$ alloys was found to be dependent on aluminum content. Alloys containing 7.8 w/o Al exhibited substantially greater resistance to cyclic thermal fatigue (400-1122°C) under stress than both D.S. Mar M200 + Hf and $\gamma/\gamma'-\delta$.

6. Superb resistance of α -Mo fibers to coarsening was demonstrated for $\gamma'/\gamma-\alpha$ alloys containing 4.7-7.8 w/o Al exposed for 1000 hrs at 1100°C.

7. The coefficient of thermal expansion of $\gamma'/\gamma-\alpha$ was found to depend on orientation (i.e. 11.2, 8.2, and $9.6 \times 10^{-6} \text{ }^\circ\text{C}^{-1}$ for transverse, longitudinal and diagonal orientations respectively). These values were below all phases of the MCrAlY coating system except α -Cr. Thus the requirement to develop a lower expansion protective coating was suggested.

8. No alloy addition or modification to $\gamma'/\gamma-\alpha$ was found that suppressed the rapid attack and oxide scale spalling due to Na₂SO₄ exposure.

REFERENCES

1. Lemkey, F. D.: "Eutectic Superalloys Strengthened by δ , Ni_3Cb Lamellae and γ' Ni_3Al Precipitates", NASA CR-2278, Nov. 1973, Contract NAS3-15562.
2. Lemkey, F. D.: "Development of Directionally Solidified Eutectic Nickel and Cobalt Alloys", Final Report NADC-76115-30, Dec. 1975, Contract N62269-75-C-0129.
3. Sheffler, K. D., R. H. Barkalow, J. J. Jackson, and A. Yuen: "Alloy and Structural Optimization of a Directionally Solidified Lamellar Eutectic A Alloy", NASA CR-135000, May 1976, Contract NAS3-17811.
4. Bruch, C.: "Eutectic Composite Turbine Blade Development", Quarterly Technical Report, #10, Dec. 1975, Contract F33615-73-C-5050 and Chang, W. H.: "Development of an In Situ Composite Alloy for High Pressure Turbine Blades", Technical Report #9, July 1976, Contract F33615-74-C-5083.
5. Curwick, L. R.: "Dispersion Strengthened High Volume Fraction γ' Ni-Cr-Al Alloys by Mechanical Alloying", 3rd Quarterly Report, April 1976, Contract N00019-75-C-0313.
6. Brentnall, W. D.: "Metal Matrix Composites for High Temperature Turbine Blades", Final Report, N62269-75-C-0119, April 1976.
7. Thompson, E. R. and E. H. Kraft: "The Response of Complex Eutectic Alloys to Directional Solidification", Final Report, Contract DAHCO4-72-C-0041, May 1975.
8. Breinan, E. M., E. R. Thompson, and F. D. Lemkey: Proc. of the Conf. on In Situ Composites, Sept. 1972, NMAB-308-II, 201.
9. Lemkey, F. D.: "Development of a Second Generation Ductile/Ductile $\gamma'/\gamma-\alpha$ Eutectic Superalloy", Proceedings of the 14th International Conference on Superalloy Processing, Sept. 12-15, 1976, Seven Springs, PA.
10. Henry, M.: Note to appear in Scripta Met., Nov. 1976.
11. Walter, J. L.: GE R&D Center, private communication.
12. Douglas, F. D.: "Processing Eutectics in Space", Contract NAS8-29669/M8, Aug. 1976.

13. Wagner, C.: Z. Electrochem, 65 (1961) p 581.
14. Lifshitz, J. M. and U. V. Slyosov: J. Phys. Chem. Solids, 19 (1961) p 35.
15. Lowell, C. E., R. G. Garlick, and B. Henry: "Thermal Expansion in the Nickel-Chromium-Aluminum and Cobalt-Chromium-Aluminum Systems to 1200°C", NASA TM X-3268, August 1975.

Table I

Purity of Charge Elements
in ppm

	Nickel ¹	Chromium H. P. Flake ²	Carbon ³	Aluminum ⁴	Cobalt ⁵	Tantalum ⁶	Molybdenum ⁷	Titanium ⁸	Rhenium ⁹	Tungsten ¹⁰	Boron ¹¹	Silicon ¹²
Al	100	<2	-	bal.	-	-	-	-	-	-	-	-
B	-	-	-	-	-	-	-	-	-	-	99.8	-
C	-	10	-	-	60	<30	10	-	-	-	-	-
Ca	-	-	-	-	-	<10	-	-	-	-	-	-
Cb	-	-	-	-	-	262	-	-	-	-	-	-
Cd	-	-	-	-	-	-	-	-	-	-	-	-
Co	-	-	-	-	-	<5	-	-	-	-	-	-
Cr	-	-	-	-	-	-	-	-	-	-	-	-
Cu	1	2	-	-	30	-	-	1	-	-	-	-
Fe	200	<2	-	2	40	<15	20	5	-	-	-	-
H	-	<60	-	-	-	5	-	-	-	-	-	-
Hf	-	-	-	-	-	-	-	-	-	-	-	-
Mg	10	-	-	2	-	<5	-	1	-	-	-	-
Mn	-	-	20	-	9	-	-	1	-	-	-	-
Mo	-	-	-	-	-	<10	-	-	-	-	-	-
N	-	<30	-	-	-	25	-	-	-	-	-	-
Ni	bal.	<30	-	-	440	<10	<10	-	-	-	-	-
O	-	<600	-	-	-	<50	-	-	-	-	-	-
Pb	-	<2	-	-	3	-	-	-	99.9 ⁺	-	-	-
Re	-	-	-	-	-	-	-	-	-	-	-	-
S	-	<30	-	-	20	-	-	-	-	-	-	-
Si	100	<10	-	-	20	<10	10	1	-	-	-	97 ⁺
Sn	-	-	-	-	-	-	-	200	-	-	-	-
Ta	-	-	-	-	-	-	-	-	-	-	-	-
Ti	-	-	-	-	-	-	-	-	-	-	-	-
V	-	-	-	-	-	<10	-	-	-	-	-	-
W	<100	-	-	-	-	140	-	-	-	99.9 ⁺	-	-
Zn	-	-	-	-	60	-	-	-	-	-	-	-
Zr	-	-	-	-	-	-	-	-	-	-	-	-

¹United Mineral & Chemical Corp.
²Shieldalloy Corp.
³Union Carbide, Spectrographic Grade
⁴Gallard Schlesinger Chemical Mfg. Corp.
⁵African Metals Corp.
⁶Wah-Chang Corp.

⁷Amax Specialty Metals
⁸Johnson Matthey Corp.
⁹Cleveland Refractory Metals
¹⁰Phillips-Elmet Corp.
¹¹United Mineral & Chemical Co.
¹²Fischer Chemical

Table II

Directional Solidification Experiments on Ternary
Modifications of $\gamma'/\gamma-\alpha$

Specimen No.	Composition	R (cm/hr)	G (°C/cm)	Microstructure
A75-787	Ni-42.3Mo-1.1Al	3	~300	$\gamma + \delta$ (primary γ)
A75-789	Ni-39.7Mo-2.5Al	↓	↓	$\gamma + \delta$ (primary γ)
A76-275	Ni-42Mo-3.0Al	↓	↓	aligned microduplex
A76-270	Ni-39.5Mo-3.5Al	↓	↓	aligned microduplex
A75-793	Ni-36.8Mo-3.7Al	↓	↓	aligned microduplex
A76-212	Ni-37.5Mo-4.0Al	↓	↓	+ primary γ
A76-289	Ni-37.5Mo-4.0Al	↓	↓	+ primary γ
A76-288	Ni-36Mo-4.7Al	↓	↓	aligned microduplex
A76-202	Ni-36Mo-4.7Al	↓	↓	aligned microduplex
A75-767	Ni-32Mo-5.0Al	↓	↓	primary γ
A76-232	Ni-35Mo-5.5Al	↓	↓	aligned microduplex
A76-238	Ni-35Mo-5.5Al	↓	↓	
A76-188	Ni-35Mo-5.5Al	↓	↓	
A76-192	Ni-35Mo-5.5Al	↓	↓	
A76-316	Ni-36Mo-5.5Al	10	↓	
A76-317	Ni-36Mo-5.5Al	25	↓	
A76-320	Ni-35Mo-5.5Al	2	↓	
A76-322	Ni-35Mo-5.5Al	2	↓	
A76-199	Ni-31.5Mo-6.2Al	3	↓	
A76-203	Ni-31.5Mo-6.2Al	3	↓	
A76-280	Ni-27.2Mo-7.8Al	3	↓	
A75-023	Ni-27.0Mo-8.0Al	3	↓	
A75-797	Ni-27.2Mo-9.0Al	3	↓	primary β/γ' + microduplex
A75-800	Ni-26.9Mo-9.8Al	3	↓	primary β/γ' + microduplex

Table III

Differential Thermal Analysis Data for Ni-Al-Mo Alloys

Composition (w/o)	Liquidus Temp (°C)	Solidus Temp (°C)	Reaction Inferred
Ni-26.9Mo-9.8Al	1303	1302	$L \rightarrow \gamma'/\beta + \alpha$
Ni-27.2Mo-9.0Al	1308	1305	$L \rightarrow \gamma' + \alpha$
Ni-27.0Mo-8.0Al	1307	1305	$L \xrightarrow{\Delta T} \gamma'/\gamma + \alpha$
Ni-31.5Mo-6.2Al	1310	1309	$L \approx \gamma/\gamma' + \alpha$
Ni-35.0Mo-5.5Al	1309	1307	$L \rightarrow \gamma/\gamma' + \alpha$
Ni-32.0Mo-5.0Al	1316	1307	$L \xrightarrow{\Delta T} \gamma/\gamma' + \alpha$ (primary γ)
Ni-34.6Mo-4.7Al	1313	1306	$L \xrightarrow{\Delta T} \gamma/\gamma' + \alpha$
Ni-36.8Mo-3.7Al	1313	1306	$L \xrightarrow{\Delta T} \gamma/\gamma' + \alpha$
Ni-39.7Mo-2.5Al	1318	1311	$L \xrightarrow{\Delta T} \gamma/\gamma' + \delta$
Ni-42.3Mo-1.1Al	1321	1314	$L \xrightarrow{\Delta T} \gamma/\gamma' + \delta$
Ni-31.5Mo-6.2Al-2.0Cr	1303	1301	$L \xrightarrow{\Delta T} \gamma/\gamma' + \alpha$
Ni-29.5Mo-6.2Al-3.0Cr	1297	1297	$L \rightarrow \gamma/\gamma' + \alpha$ or $\gamma + \gamma' + \alpha$
Ni-29.0Mo-6.2Al-6.0Cr	1292	1288	$L \xrightarrow{\Delta T} \gamma/\gamma' + \alpha$
Ni-27.5Mo-6.2Al-9Cr	1283	1278	$L \xrightarrow{\Delta T} \gamma/\gamma' + \alpha$

Table IV

Directional Solidification Experiments on Quaternary and Higher Order System Modifications

<u>Specimen No.</u>	<u>Composition</u> (w/o)	<u>R</u> (cm/hr)	<u>G</u> (°C/cm)	<u>Microstructure</u>		
<u>Chromium Modifications</u>						
A76-061	Ni-34Mo-5.5Al-1.0Cr	2	-300	N ₂ atmosphere		
A76-243	Ni-34Mo-5.5Al-1.0Cr	2	↓	A atmosphere		
A76-323	Ni-31Mo-6.2Al-1.0Cr	10		A atmosphere		
A76-191	Ni-34Mo-5.5Al-2.0Cr	3		A atmosphere		
A76-245	Ni-34Mo-5.5Al-2.0Cr			A atmosphere		
A76-206	Ni-31Mo-6.2Al-2.0Cr	↓		A atmosphere		
A76-065	Ni-33Mo-5.5Al-3.0Cr			N ₂ atmosphere		
A76-187	Ni-34Mo-5.5Al-3.0Cr			A atmosphere		
A76-200	Ni-31Mo-6.2Al-3.0Cr			A atmosphere		
A76-236	Ni-34Mo-5.5Al-3.0Cr			A atmosphere		
A76-240	Ni-34Mo-5.5Al-3.0Cr			A atmosphere		
A76-255	Ni-34Mo-5.5Al-3.0Cr			A atmosphere		
A76-264	Ni-34Mo-5.5Al-3.0Cr			A atmosphere		
A76-265	Ni-34Mo-5.5Al-3.0Cr			A atmosphere		
A76-266	Ni-34Mo-5.5Al-3.0Cr			A atmosphere		
A76-257	Ni-34Mo-5.5Al-4.0Cr			A atmosphere		
A76-182	Ni-34Mo-5.5Al-4.0Cr			N ₂ atmosphere		
A76-195	Ni-31Mo-6.2Al-4.0Cr			A atmosphere		
A76-068	Ni-32Mo-5.5Al-6.0Cr			↓	A atmosphere	
<u>Cobalt Modifications</u>						
A76-038	Ni-35Mo-5.5Al-1Co			3	-300	Aligned microduplex
A76-042	Ni-35Mo-5.5Al-3Co		↓	↓	Aligned microduplex	
A76-044	Ni-35Mo-5.5Al-7Co				Aligned microduplex	
A76-047	Ni-35Mo-5.5Al-9Co	New phases				
<u>Iron Modifications</u>						
A76-036	Ni-35Mo-5.5Al-5.0Fe	3	-300	Aligned microduplex		
<u>Rhenium Modifications</u>						
A76-174	Ni-33Mo-5.5Al-3.0Re	2	-300	Aligned microduplex		
<u>Tantalum Modifications</u>						
A76-056	Ni-32Mo-5.5Al-1Ta	3	~300	Aligned microduplex		
A76-048	Ni-32Mo-5.5Al-3Ta			Aligned microduplex		
A76-035	Ni-32Mo-5.5Al-5Ta			Primary γ/γ'		
A76-039	Ni-32Mo-5.5Al-7Ta			Primary γ/γ'		
A76-052	Ni-32Mo-5.5Al-9Ta			Primary γ/γ'		
A76-074	Ni-33Mo-3.0Cr-2.0Ta-2.5Ti-3.0Al			Cellular		
A76-267	Ni-32Mo-5.5Al-1Ta-3Cr			Cellular		
A76-272	Ni-32Mo-5.5Al-1Ta-3Cr-0.066C			↓	Ternary eutectic (cellular)	
A76-284	Ni-32Mo-5.5Al-1Ta-3Cr-0.066C			2	↓	Ternary eutectic (cellular)
<u>Titanium Modifications</u>						
A76-051	Ni-32Mo-5.5Al-1.5Ti	3	~300	Cellular & new phases		
A76-071	Ni-33Mo-3.0Al-3.0Cr-2.5Ti	3	-300	Cellular microduplex		
<u>Tungsten Modifications</u>						
A76-299	Ni-32Mo-5.5Al-1.0W	2	~300	Aligned microduplex		
A76-301	Ni-34Mo-5.5Al-1.0W-3Cr	2	-300	Aligned microduplex		
A76-314	Ni-29Mo-5.5Al-3W	2	-300	Primary γ'/γ		

Table V

Composition of Extracted α Mo Fibers from $\gamma'/\gamma-\alpha$
Alloys Containing 6.2 w/o

<u>Specimen No.</u>	<u>w/o Cr in $\gamma'/\gamma-\alpha$</u>	<u>w/o Al in α</u>	<u>w/o Ni in α</u>	<u>w/o Cr in α</u>
A76-203	0	0.38	1.7	0
A76-243	1	0.20	2.26	0.47
A76-749	2	0.36	1.37	0.91
A76-200	3	0.19	1.69	1.69
A76-195	4	0.22	1.23	2.56
A75-758	5	0.27	1.53	2.58
A75-831	6	0.16	1.33	3.59
A75-753	9	0.26	1.76	7.19

Table VI

Interfiber Spacing Measurements of Modified γ/γ' - α Alloys
Directionally Solidified at $R = 3$ cm/hr, $G_L \sim 300^\circ\text{C}/\text{cm}$

<u>Specimen No.</u>	<u>Alloy Composition w/o</u>	<u>N</u>	<u>$A(\mu)^2$</u>	<u>$\bar{\lambda}(\mu)$</u>
A76-238-02	Ni-35Mo-5.5Al	1655	2500	1.23
A76-056-02	Ni-32Mo-5.5Al-1Ta	1096	2500	1.51
A76-267-01	Ni-32Mo-5.5Al-1Ta-3Cr	1333	2500	1.37
A76-048-04	Ni-32Mo-5.5Al-3Ta	1314	2500	1.38
A76-299-01	Ni-32Mo-5.5Al-1W	908	2500	1.66
A76-301-01	Ni-34Mo-5.5Al-1W-3Cr	1229	2500	1.43
A76-202-02	Ni-36Mo-4.7Al	1297	2500	1.39

Table VII

Stress Rupture Tests of Modified γ'/γ - α Alloys Performed In Air

Specimen No.	Composition (w/o)	R (cm/hr)	G (°C/cm)	T (°F)	σ (ksi)	t_r (hrs)	% RA	% Elong.
<u>Aluminum Modifications</u>								
A76-289-01	Ni-37.5Mo-4.0Al	3	-300	1900	30	43.9	76.7	18.8
A76-212-01	Ni-37.5Mo-4Al	↓	↓	1900	30	27.5	51.4	14.0
A76-212-02	Ni-37.5Mo-4Al	↓	↓	1400	120	298.3	15.9	5.6
A76-202-02	Ni-36Mo-4.7Al	↓	↓	1900	30	110.7	53.4	11.4
A76-202-03	Ni-36Mo-4.7Al	↓	↓	1400	120	287.4	34.8	15.6
A76-238-02	Ni-35Mo-5.5Al	↓	↓	1900	30	96.1	50.2	14.8
A76-317-03	Ni-36Mo-5.5Al	10	↓	1900	30	11.0	13.4	36.3
A76-316-03	Ni-36Mo-5.5Al	10	↓	1400	120	139.3	9.6	24.1
A76-199-01	Ni-31.5Mo-6.2Al	3	↓	1900	30	121.3	48.9	25.8
A76-131-01	Ni-31.5Mo-6.2Al	1.5	↓	2039	25	23.2	65.1	18.1
<u>Chromium Additions</u>								
A76-243-02	Ni-34.0Mo-5.5Al-1Cr	3	-300	1900	30	108.7	33.3	9.4
A76-243-03	Ni-34Mo-5.5Al-1Cr	3	↓	1400	120	151.3	47.2	26.0
A76-323-02	Ni-31Mo-6.2Al-1.0Cr	10	↓	1900	30	26.5	48.9	23.0
A76-323-03	Ni-31Mo-6.2Al-1.0Cr	10	↓	1900	30	19.9	53.6	24.1
A76-245-02	Ni-34.0Mo-5.5Al-2Cr	3	↓	1900	30	94.6	37.3	12.8
A76-245-03	Ni-34.0Mo-5.5Al-2Cr	↓	↓	1400	120	177.7	50.2	23.8
A76-206-01	Ni-31Mo-6.2Al-2Cr	↓	↓	1900	30	68.7	12.4	44.8
A76-206-02	Ni-31Mo-6.2Al-2Cr	↓	↓	2039	25	33.5	41.9	17.4
A76-251-02	Ni-34.0Mo-5.5Al-3Cr	↓	↓	1900	30	62.2	19.2	10.2
A76-251-03	Ni-34.0Mo-5.5Al-3Cr	↓	↓	1400	120	127.8	47.5	31.8
A76-264-03	Ni-34.0Mo-5.5Al-3Cr	↓	↓	1900	30	109.3	46.2	20.8
A76-264-02	Ni-34.0Mo-5.5Al-3Cr	↓	↓	1900	30	43.5	22.5	7.0
A76-240-03	Ni-34.0Mo-5.5Al-3Cr	↓	↓	1900	30	54.0	40.6	11.4
A76-240-02	Ni-34.0Mo-5.5Al-3Cr	↓	↓	1900	30	111.6	44.8	18.8
A76-255-02	Ni-34.0Mo-5.5Al-3Cr	↓	↓	1900	30	51.7	28.8	13.8
A76-255-03	Ni-34.0Mo-5.5Al-3Cr	↓	↓	1400	120	182.8	41.0	24.1
A76-195-02	Ni-31.0Mo-6.2Al-4Cr	↓	↓	1900	30	33.7	52.6	20.2
A76-257-03	Ni-34Mo-5.5Al-4Cr	↓	↓	1900	30	62.9	9.4	22.4
A76-257-02	Ni-34Mo-5.5Al-4Cr	↓	↓	1900	30	3.7	12.4	4.6
A76-257-01	Ni-34.0Mo-5.5Al-4Cr	↓	↓	1900	30	44.6	52.6	27.6
A76-257-03	Ni-34.0Mo-5.5Al-4Cr	↓	↓	1900	30	62.9	22.4	9.4
<u>Cobalt Additions</u>								
A76-042-03T	Ni-35Mo-5.5Al-3Co	3	-300	1400	20	128.4	24.0	16.1
A76-042-01H	Ni-35Mo-5.5Al-3Co	↓	↓	1900	30	36.3	22.4	9.2
A75-893-02	Ni-35Mo-5.5Al-5Co	↓	↓	1900	30	32.0	31.6	12.6
A75-893-03	Ni-35Mo-5.5Al-5Co	↓	↓	1400	115	89.9	23.8	20.2
A76-044-02	Ni-35Mo-5.5Al-7Co	↓	↓	1900	30	0.9	64.4	27.1
<u>Iron Additions</u>								
A76-036-03	Ni-35Mo-5.5Al-5Fe	3	-300	1900	30	70.5	43.4	20.7

Table VII (Cont'd)

<u>Specimen No.</u>	<u>Composition</u> (w/o)	<u>R</u> (cm/hr)	<u>G</u> (°C/cm)	<u>T</u> (°F)	<u>σ</u> (ksi)	<u>t_r</u> (hrs)	<u>% RA</u>	<u>% Elong.</u>
<u>Tantalum Additions</u>								
A76-056-01H	Ni-32Mo-5.5Al-1Ta	3	~300	1900	30	135.4	51.3	33.3
A76-056-03T	Ni-32Mo-5.5Al-1Ta	↓	↓	1400	120	283.3	33.3	20.9
A76-267-01	Ni-32Mo-5.5Al-1Ta-3Cr	↓	↓	1900	30	84.4	9.3	33.7
A76-369-01	Ni-32Mo-5.5Al-2Ta	↓	↓	1900	30	107.4	52.6	13.7
A76-369-02	Ni-32Mo-5.5Al-2Ta	↓	↓	1900	30	108.9	37.8	7.9
A76-371	Ni-32Mo-5.5Al-2Ta-3Cr	↓	↓	1900	30	33.3	26.0	5.2
A76-048-01H	Ni-32Mo-5.5Al-3Ta	↓	↓	1900	30	73.9	42.0	21.1
A76-048-03T	Ni-32Mo-5.5Al-3Ta	↓	↓	1400	120	230.4	40.6	33.3
A75-934-01	Ni-33Mo-5.5Al-4Ta	↓	↓	1900	30	9.9	20.8	17.9
A75-934-02	Ni-33Mo-5.5Al-4Ta	↓	↓	1400	120	86.0	27.0	16.5
<u>Rhenium & Tungsten Additions</u>								
A75-867-02	Ni-30Mo-6.2Al-3Re	2	~300	1900	30	163.7	57.2	26.0
A76-299-01	Ni-32Mo-5.5Al-1W	2	~300	1900	30	136.2	22.2	66.9
A76-301-01	Ni-34Mo-5.5Al-1W-3Cr	2	~300	1900	30	51.5	11.4	46.2

Table VIII

Stress Rupture Tests on Transversely Oriented $\gamma'/\gamma-\alpha$
(Ni-31.5 w/o Mo-6.2 w/o Al) in Air

<u>Specimen No.</u>	<u>Temp (°F)</u>	<u>σ (ksi)</u>	<u>t_r (hrs)</u>	<u>R.A. (%)</u>	<u>Elong. (%)</u>	<u>LMP</u>
E-591-1 trans	1400	65	141.5	5.5	3.6	41.2
E-591-2 trans	1400	70	81.3	3.6	2.9	40.8
E-591-3 trans	1600	40	23.5	9.0	4.4	44.0
E-591-4 trans	1800	22	10.3	-	5.0	47.5
E-591-5 trans	1900	14	12.8	2.0	4.2	49.8
E-591-6 trans	1900	12	21.9	-	3.8	50.4
E-591-7 trans	2000	10	7.2	1.8	2.2	51.3
E-591-8 trans	2000	8	19.6	9.1	2.4	52.4

Table IX

Temperature Dependence of Ultimate Shear Strength from Bolt Head Tensile Tests of D.S. $\gamma'/\gamma-\alpha$ Alloys

Specimen No.	Composition (w/o)	R cm/hr	Shear Strength, psi		Fracture Mode
			1400°F (760°C)	1600°F (870°C)	
A75-506-01	Ni-27.2Mo-7.8Al	25	98,000	-	Mixed
A75-506-02	Ni-27.2Mo-7.8Al	25	-	52,300	Shear
A76-203-01	Ni-31.5Mo-6.2Al	3	79,500	-	Shear
A76-203-02	Ni-31.5Mo-6.2Al	3	-	65,200	Shear
A76-232-01	Ni-35Mo-5.5Al	3	80,600	-	Shear
A76-232-02	Ni-35Mo-5.5Al	3	-	66,300	Shear
A76-243-01	Ni-34Mo-5.5Al-1Cr	3	108,300	-	Shear
A76-206-01	Ni-31Mo-6.2Al-2Cr	3	95,500	-	Shear
A76-236-01	Ni-34Mo-5.5Al-3Cr	3	103,200	-	Shear
A76-236-02	Ni-34Mo-5.5Al-3Cr	3	-	62,800	Shear
PWA 663	B-1900	cc	~97,500	72,000	-
$\gamma/\gamma'-\delta^*$	Ni-20Cr-6Cr-2.5Al	3	48,300	37,700	Shear
$\gamma/\gamma'-\delta^*$	Ni-20Cr-6Cr-2.5Al	3	49,200	39,400	Shear

*Heat treatment of 1975°F (4 hrs) + 1650°F (24 hrs)

Table X

Double Bolt Head Shear Rupture Specimens Tested in Air

<u>Specimen No.</u>	<u>Composition</u> <u>w/o</u>	<u>R</u> <u>(cm/hr)</u>	<u>T</u> <u>(°F)</u>	<u>τ</u> <u>(ksi)</u>	<u>t_r</u> <u>(hrs)</u>
A76-188	Ni-35Mo-5.5Al	3	1400	25	208.7
A76-232-02	Ni-35Mo-5.5Al	3	1400	30	113.8
A76-203-02	Ni-31.5Mo-6.2Al*	3	1400	30	127.1
A76-316-01	Ni-36Mo-5.5Al	10	1400	25	92.5
A76-316-02	Ni-36Mo-5.5Al	10	1400	30	28.8
A76-323-01	Ni-31Mo-6.2Al-1.0Cr	10	1400	30	122.4
A76-206	Ni-31Mo-6.2Al-2.0Cr	3	1400	30	167.2
A76-236-01	Ni-34Mo-5.5Al-3.0Cr	3	1400	30	274.5

Iosipescu Type Shear Specimens (P&WA)

E203-7	Ni-20Nb-6Cr-2.5Al	1.3	1300	25	>3600**
E203-8	↓	↓	1300	25	1635.8
E508D	↓	↓	1600	12	216.3
E508F	↓	↓	1600	12	379.9
B-1900			1300	70	283.4
B-1900			1300	70	325.0
B-1900			1600	25	107.0
B-1900			1600	25	107.3

*Heat treated (2050°F) (4 hrs) + (1650°F) (24 hrs)

**Discontinued

Table XI

Thermal Fatigue Test Results
2 min Cycles 750°F-2050°F (400-1122°C)

Unloaded			Loaded				
Specimen No.	Composition w/o	($\Delta l/l$) after 3000 Ω	Specimen No.	Composition w/o	σ (ksi)	Ω to Fracture	% Red. Area
A76-320-01	Ni-35Mo-5.5Al	-0.031	A76-320-02	Ni-35Mo-5.5Al	10	539 ¹	56.8
A76-322-01	Ni-35Mo-5.5Al	-0.014	A76-320-02	Ni-35Mo-5.5Al	10	1114	71.1
A76-380-02	Ni-31.5Mo-6.2Al	-0.041	A76-380-01	Ni-31.5Mo-6.2Al	10	1153	23.5
A76-393-01	Ni-27.2Mo-7.8Al	+0.001	A76-379-01	Ni-31.5Mo-6.2Al	15	597	68.6
A76-397-01	Ni-20Cb-6.0Cr-2.5Al		A76-391-02	Ni-27.2Mo-7.8Al	11-14 ²	>3000*	23.5
PWA 1422	DS MM200 + Hf	-	A76-391-01	Ni-27.2Mo-7.8Al	10	>3000*	14.4
			A76-397-01	Ni-20Cb-6.0Cr-2.5Al	10	784	3.7
			A76-397-02	Ni-20Cb-6.0Cr-2.5Al	10	1863	
			PWA 1422	DS MM200 + Hf	10	137	16.3
			PWA 1422	DS MM200 + Hf	5	1157	33.0

¹Thermocouple weld induced failure
²1500 Ω @ 11 ksi & 1500 Ω @ 14.4 ksi

*no failure

Table XII

Average Coefficient of Thermal Expansion
for γ'/γ - α as a Function of Temperature

(Ni-31.5Mo-6.2Al)

$^{\circ}\text{C}$	Transverse $\frac{\text{Avg } \alpha}{10^{-6} \text{ } ^{\circ}\text{C}^{-1}}$	Longitudinal $\frac{\text{Avg } \alpha}{10^{-6} \text{ } ^{\circ}\text{C}^{-1}}$	Diagonal (45°) $\frac{\text{Avg } \alpha}{10^{-6} \text{ } ^{\circ}\text{C}^{-1}}$
100-200	11.2	8.2	9.6
200-300	11.5	9.6	10.6
300-400	12.0	10.5	11.2
400-500	12.5	11.3	12.0
500-600	12.0	11.4	12.0
600-700	13.7	11.6	12.6
700-800	16.0	12.3	14.8
800-900	16.5	13.0	15.8
900-1000	19.3	14.5	16.3

Table XIII
 Thermogravimetric Results of 2 Hour Cyclic Oxidation at 700°C (1290°F)

	Cumulative Weight Change (mg/cm ²)														
	2	4	6	8	10	12	14	16	18	20	22	24	26	28	30
A76-200 Long Ni-31Mo-6.2Al-3Cr	0	0.05	0.04	0.04	0.04	0.04	0.04	0.05	0.05	0.03	0.04	0.01	0.01	0.02	0
A76-200 Trans Ni-31Mo-6.2Al-3Cr	0.06	0.02	0.02	0	0	0	0	0	0	0	0.01	0	0	-0.04	-0.07
A76-289-03 Ni-37.5Mo-4Al	0.07	0.13	0.14	0.16	0.18	0.17	0.18	0.18	0.18	0.23	0.30	0.30	0.23	0.30	0.26
A76-299-04 Ni-32Mo-5.5Al-1W	0.11	0.15	0.21	0.19	0.23	0.25	0.25	0.25	0.25	0.31	0.31	0.31	0.27	0.34	0.34
A76-267-03 Ni-32Mo-5.5Al-1Ta-3Cr	0.04	0.11	0.15	0.12	0.14	0.14	0.15	0.15	0.15	0.18	0.18	0.14	0.15	0.22	0.11

Note: - sign => wt. loss

Table XIV

Thermogravimetric Results of Cyclic Oxidation at 1000°C (1830°F)

Sample No.	Cumulative Weight Change (mg/cm ²) - hours														
	2	4	6	8	10	12	14	16	18	20	22	24	26	28	30
E-591 Trans Ni-31.5Mo-6.2Al	-0.52	-1.68	-3.34	-4.88	-6.71	-8.23	-10.00	-12.10	-13.91	-15.84	-17.85	-19.66	-21.73	-23.82	-25.44
E-591 Long Ni-31.5Mo-6.2Al	-0.48	-1.34	-2.41	-3.78	-5.39	-7.23	-9.45	-11.47	-13.13	-15.49	-17.53	-19.38	-21.26	-23.11	-24.97
A76-200 Long Ni-31Mo-6.2Al-3Cr	+0.14	-0.13	-0.16	-0.47	-0.55	-0.62	-0.66	-0.78	-0.88	-0.92	-1.07	-1.39	-1.47	-1.56	-1.68
A76-200 Trans Ni-31Mo-6.2Al-3Cr	+0.05	-0.26	-0.10	-0.31	-0.49	-0.70	-0.79	-0.89	-0.93	-1.21	-1.20	-1.33	-1.42	-1.59	-1.66
A76-289-03 Ni-37.5Mo-4Al	-0.93	-2.73	-5.11	-7.61	-10.09	-12.39	-14.57	-16.91	-19.29	-21.74	-24.09	-26.47	-28.67	-31.26	-33.73
A76-299-04 Ni-32Mo-5.5Al-1W	-0.19	-1.82	-3.14	-5.32	-7.15	-9.07	-11.03	-13.07	-15.07	-17.05	-19.01	-20.91	-22.74	-25.02	-27.10
A76-267-03 Ni-32Mo-5.5Al-1Ta-3Cr	+0.01	+0.09	+0.02	+0.03	+0.03	-0.26	-0.01	-0.02	-0.23	-0.29	-0.31	-0.48	-0.62	-0.71	-0.85
E-1900 Ni-0.1C-8.0Cr-10Co- 6Mo-4Ta-1Ti-6Al-0.015B- 0.1Zr	+0.14	+0.25	+0.29	+0.33	+0.33	+0.36	+0.40	+0.40	+0.37	+0.36	+0.35	+0.33	+0.34	+0.32	+0.32

Note: - sign => wt. loss

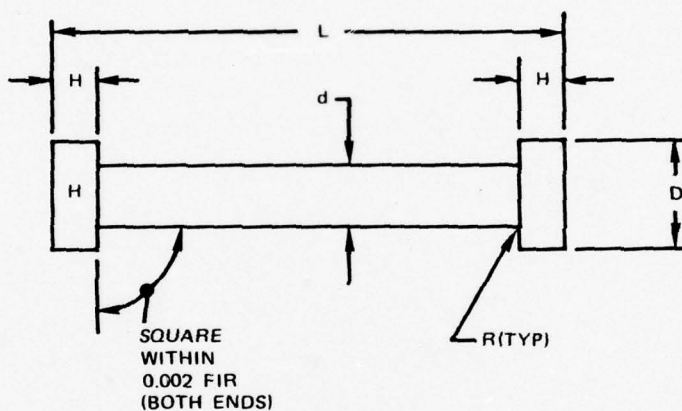
Table XV

Results of 900°C Cyclic Corrosion

<u>Sample No.</u>	<u>Weight Change (mg/cm²) after 2 Cycles</u>
E-591 Trans Ni-31.5Mo-6.2Al	-50.28
E-591 Long Ni-31.5Mo-6.2Al	-46.69
A76-200 Long Ni-31Mo-6.2Al-3Cr	-39.99
A76-200 Trans Ni-31Mo-6.2Al-3Cr	No sample run
A76-289-03 Ni-37.5Mo-4Al	-42.03
A76-299-04 Ni-32Mo-5.5Al-1W	-30.83
A76-267-03 Ni-32Mo-5.5Al-1Ta-3Cr	-24.66
B-1900 Ni-0.1C-8Cr-10Co-6Mo-4Ta-1Ti- 6Al-0.15B-0.1Zr	+ 2.88

- sign => wt. loss

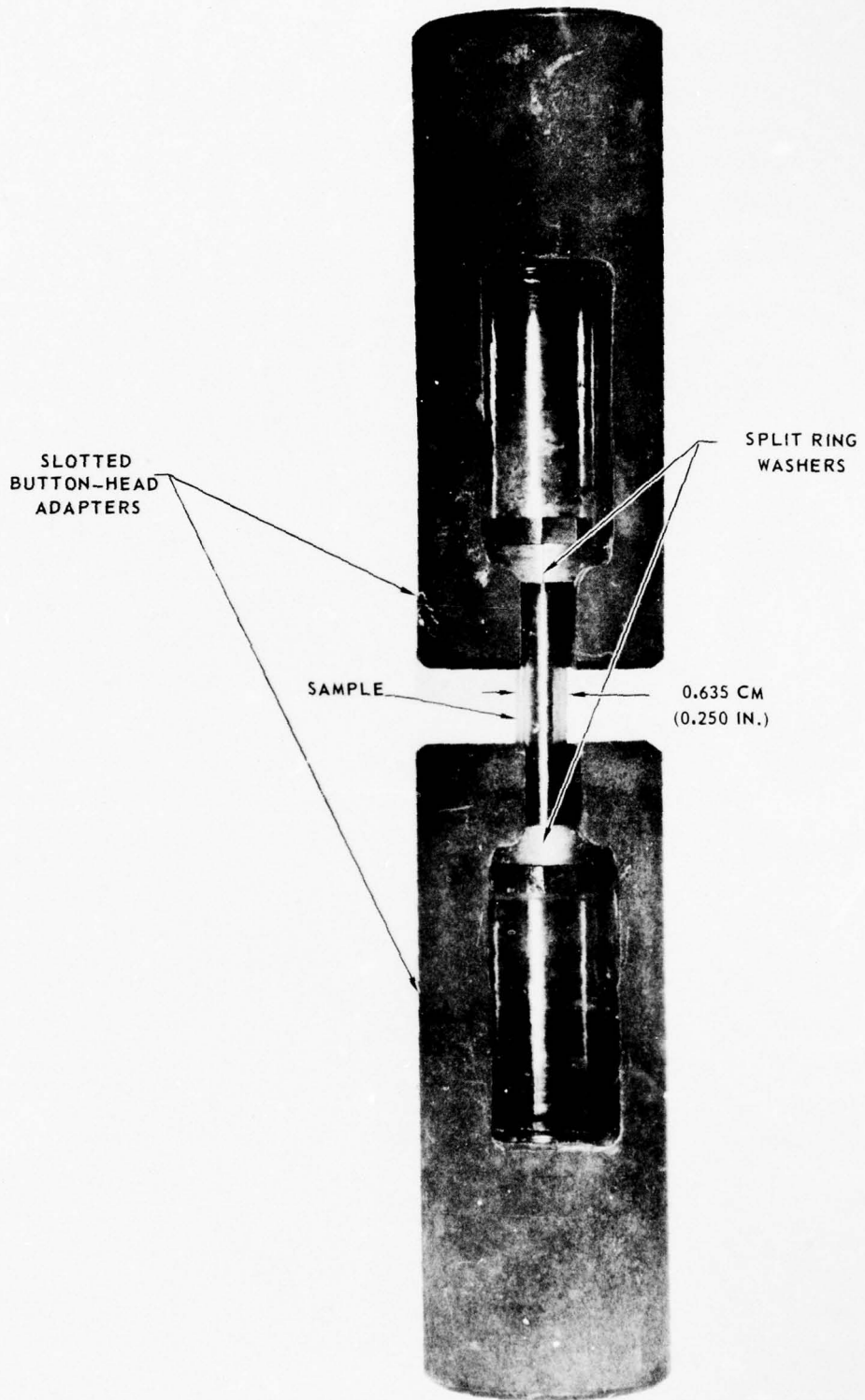
LONGITUDINAL SHEAR SPECIMEN



L	AS IS	AS IS
H	0.125 ^{+0.005} / _{-0.000}	3.18 mm ^{+0.013} / _{-0.000}
D	AS IS (1/2 IN. DIA. MAX)	12.7 mm
d	0.250 ^{+0.002} / _{-0.000} DIA	6.36 mm ^{+0.005} / _{-0.000}
FR	0.020 ^{0.015} IN.	0.051 mm ^{0.038} mm

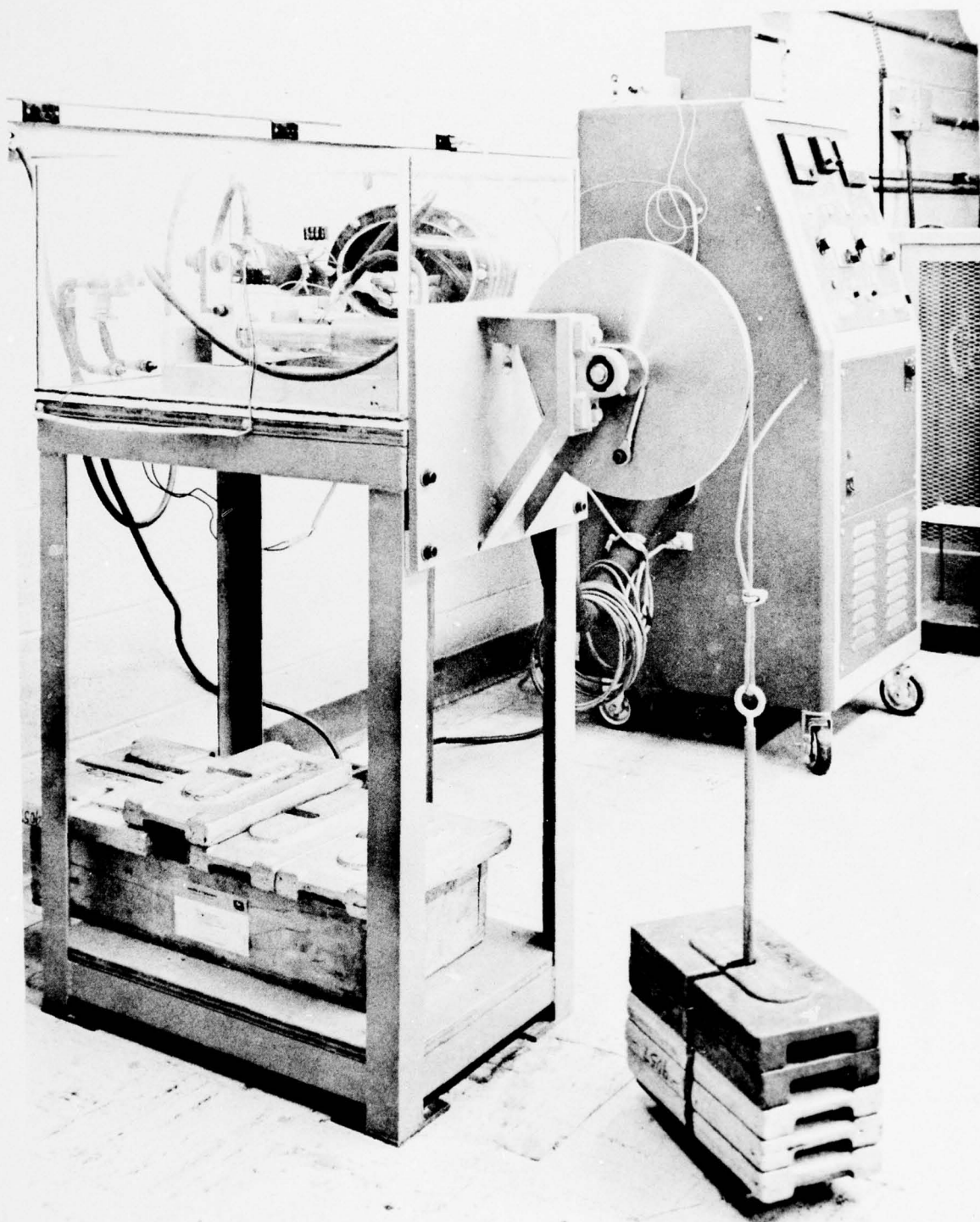
LONGITUDINAL SHEAR FIXTURE

FIG. 2

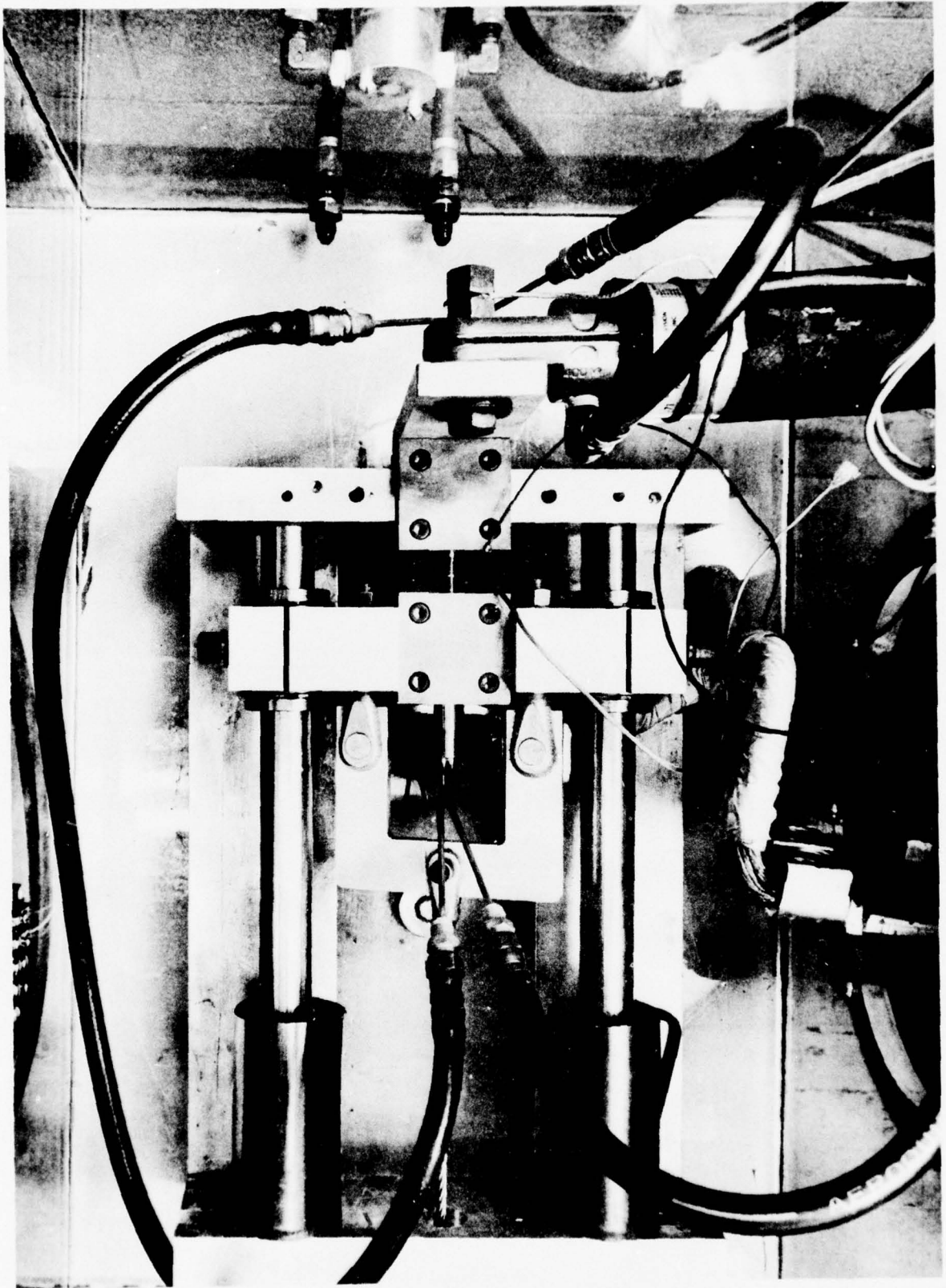


RL-71-243

THERMAL CYCLING APPARATUS



a. OVERALL VIEW



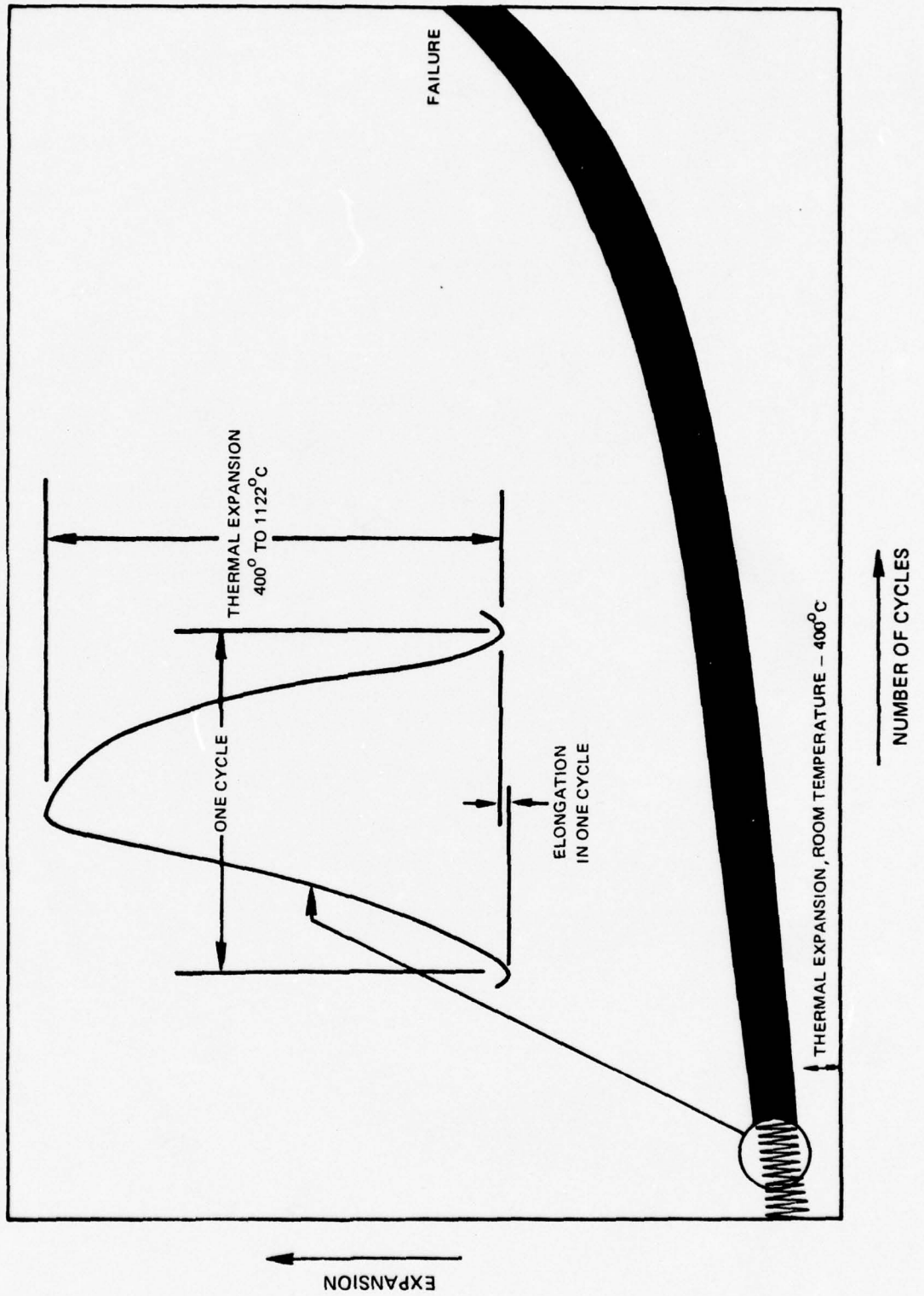
b. OVERHEAD VIEW OF SPECIMEN STAGE

RL-74-23-A

N12-154-2

FIG. 4

SPECIMEN EXPANSION DURING THERMAL CYCLING UNDER STRESS



**DIFFERENTIAL THERMAL ANALYSIS TRACE OF 61.3 w/o Ni, 29.5 w/o Mo,
6.2 w/o Al, 3.0 w/o Cr**

(HEATING RATE: 3°C/min)

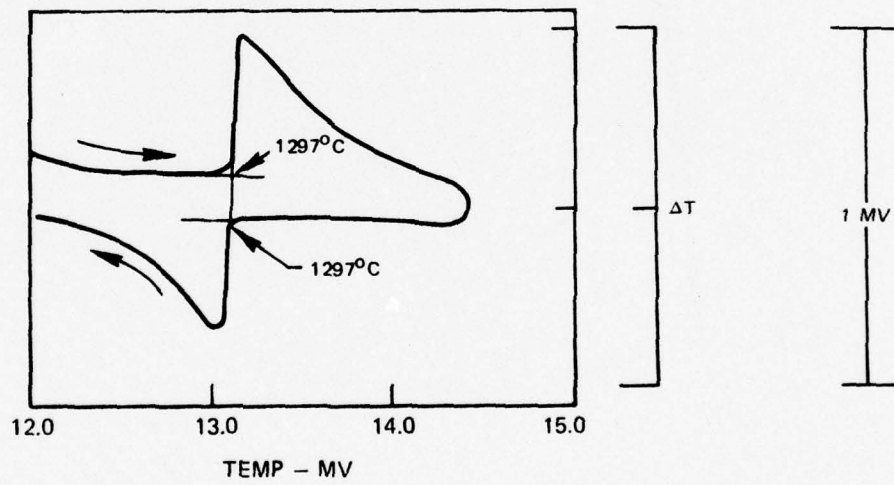
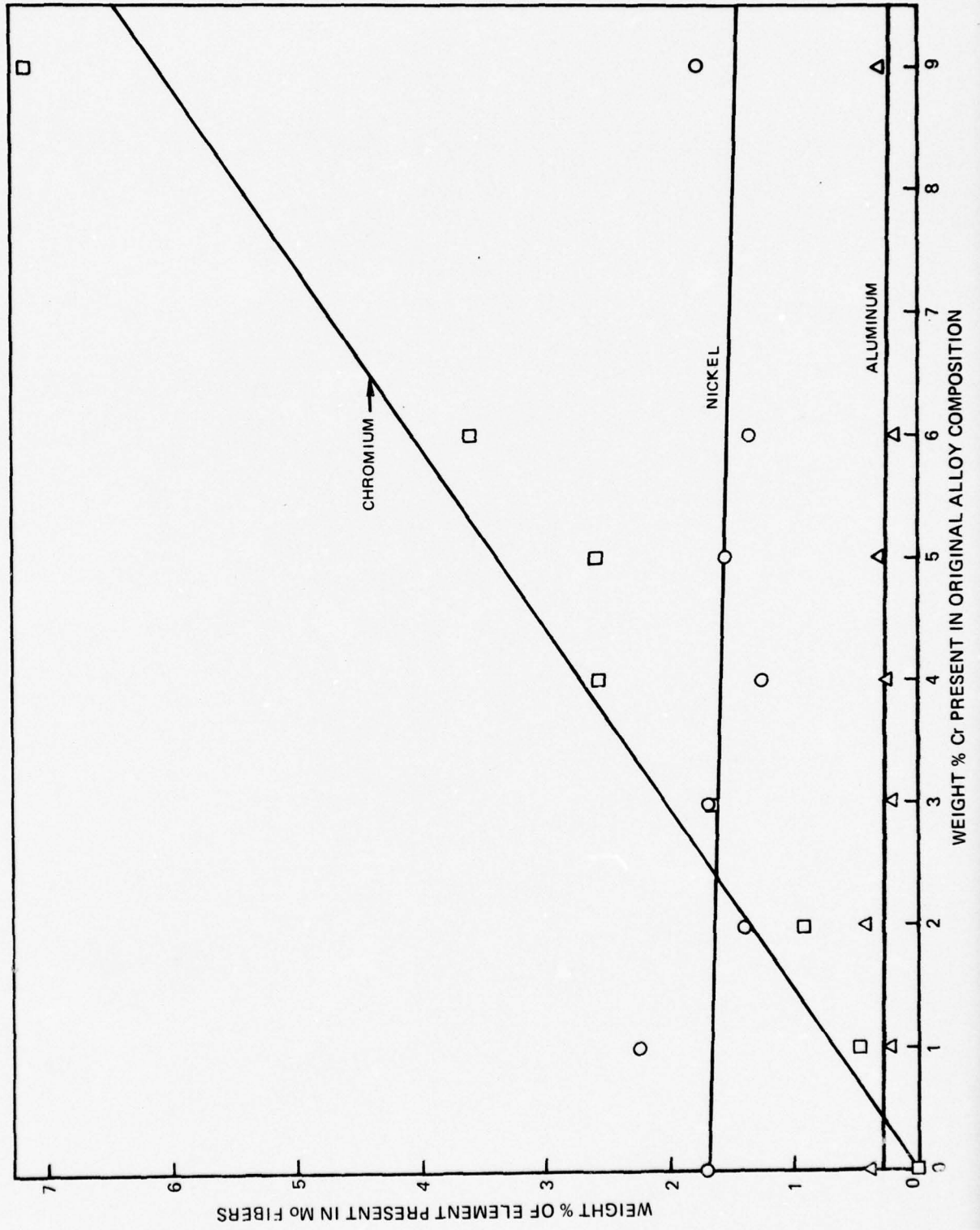
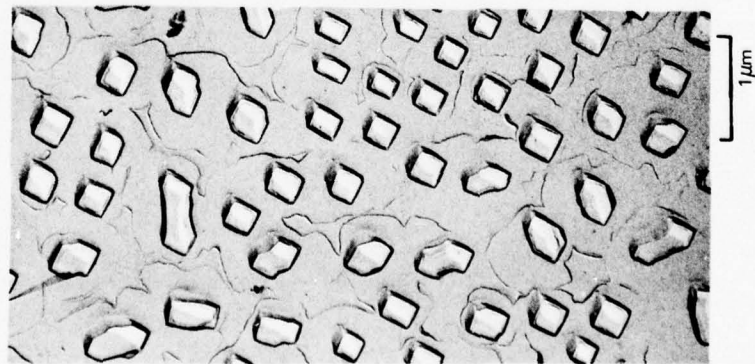


FIG. 6

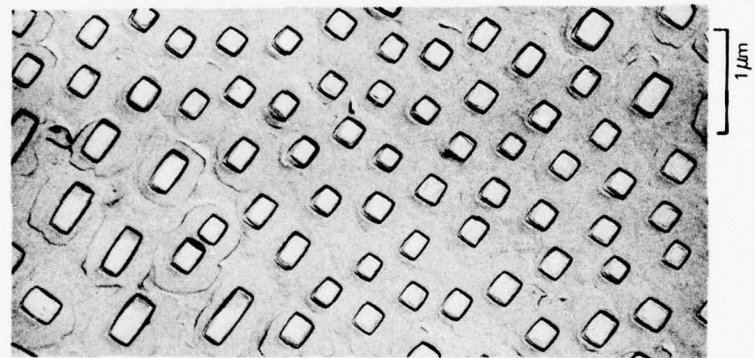
SOLUBILITY OF Cr, Ni, AND Al IN EXTRACTED Mo FIBERS FROM D. S. γ/γ' -a ALLOYS



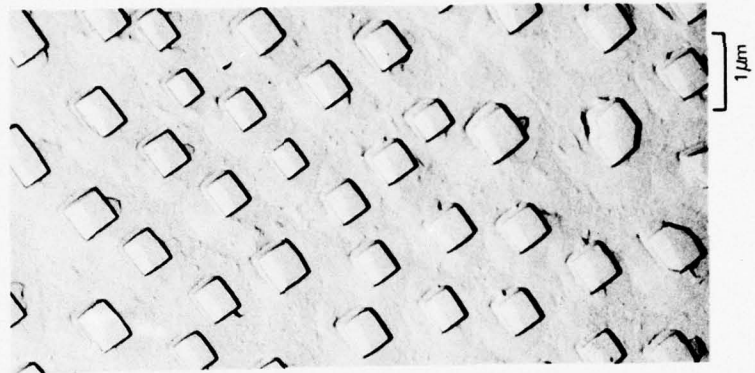
EXAMPLES OF QUARTERNARY ALLOY SUBSTITUTION TO $\gamma/\gamma - \alpha$ (Ni 32 w/o Mo-5.5 w/o Al) FOR PLANE FRONT
SOLIDIFICATION AT G/R~100°C HR CM⁻²



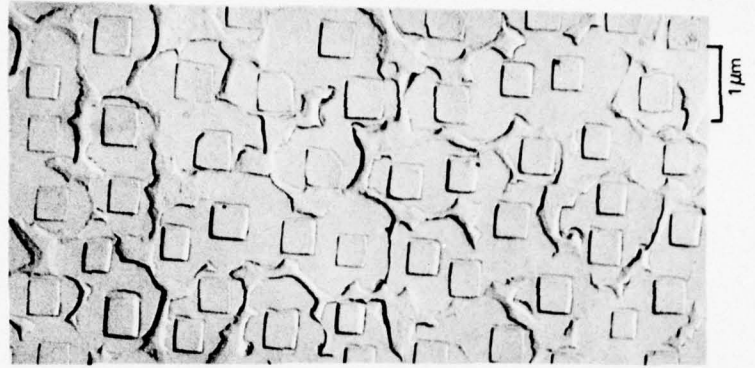
+1.5 w/o Ti



+3 w/o Ta



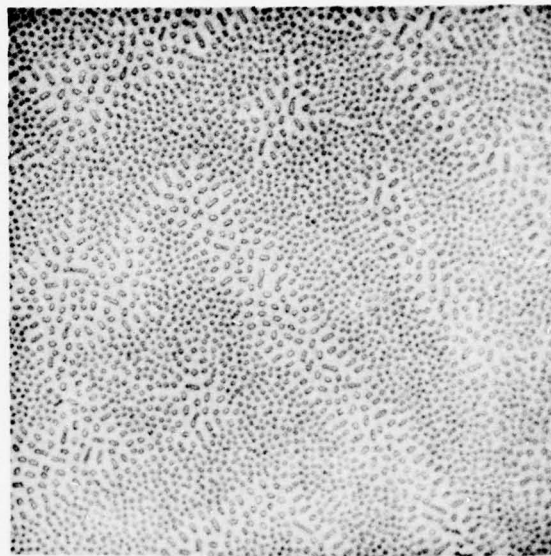
+5 w/o Fe



+7 w/o Co

ONSET OF CELLULAR MICROSTRUCTURE IN Ta MODIFIED $\gamma/\gamma-\alpha$ ALLOYS

(R = 3 cm/hr; $G_L \sim 300^\circ\text{C/cm}$)



BIMODAL α [Ni-32 w/o Mo-5.5 w/o Al-3 w/o Ta]



CELLULAR α [Ni-32 w/o Mo-5.5 w/o Al-5.0 w/o Ta]

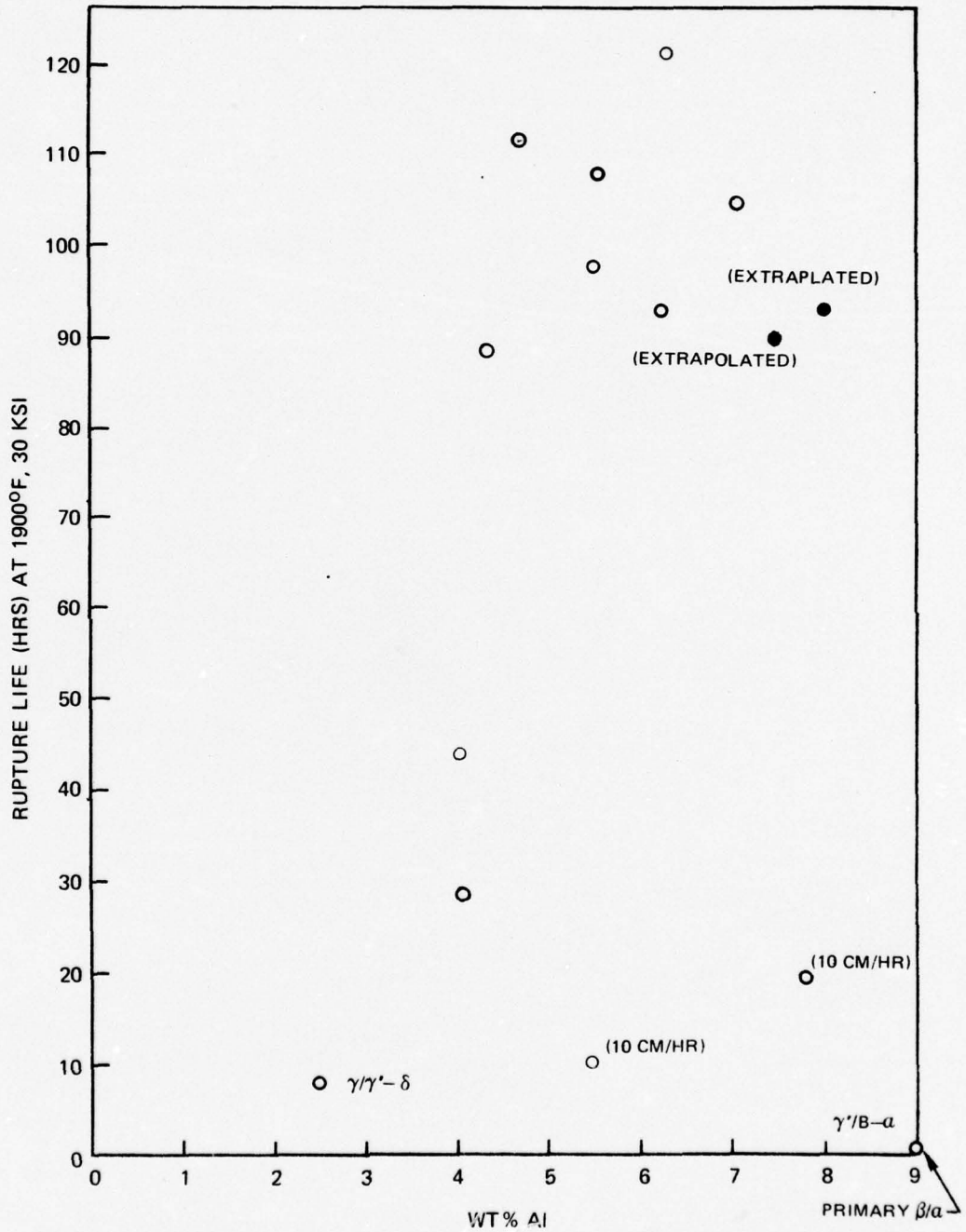
REPLICA OF TRANSVERSE SECTION OF Ni-32 w/o Mo-5.5 w/o Al-1 w/o Ta -3 w/o Cr - 0.066 w/o C



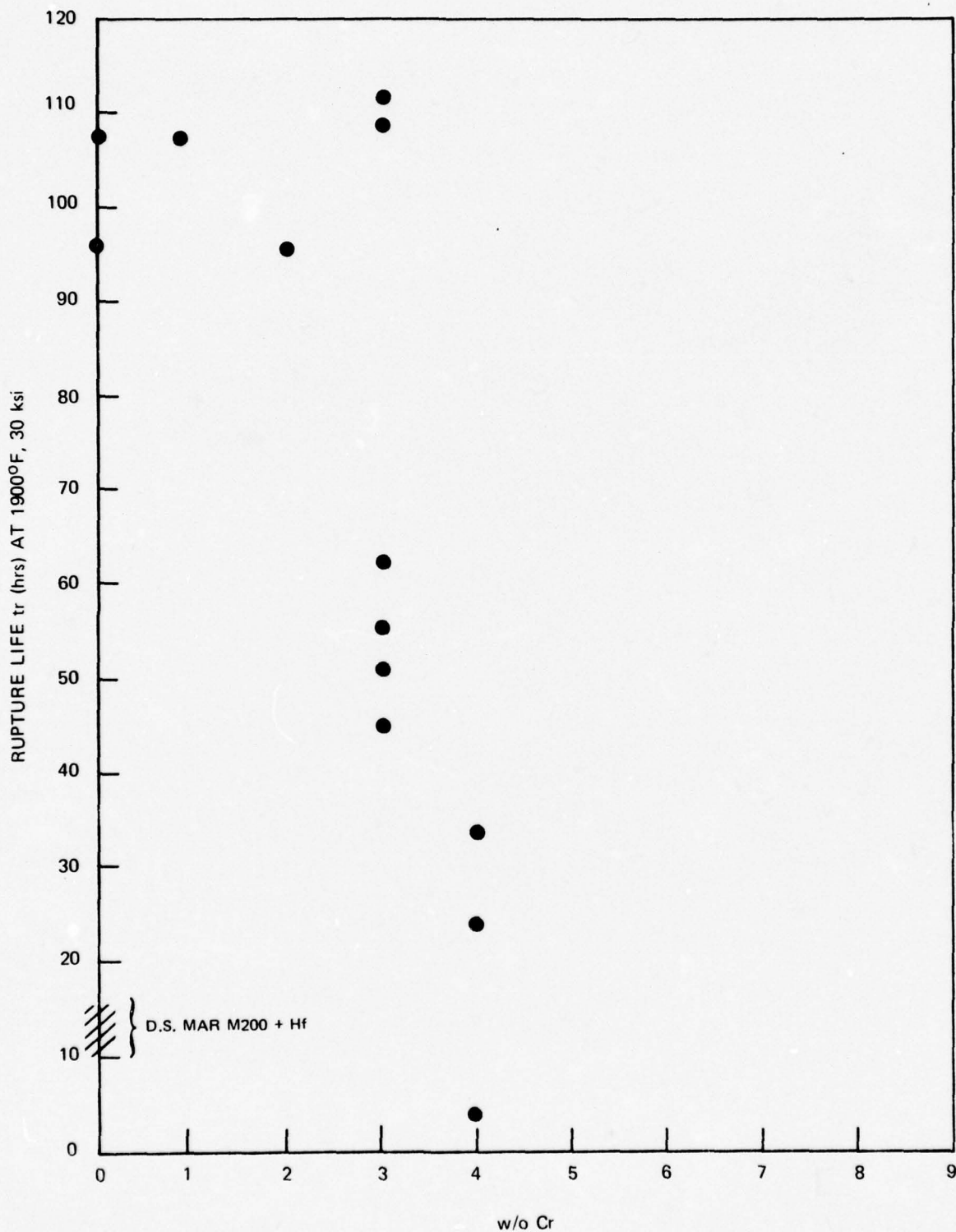
ELECTRON TRANSMISSION MICROGRAPH OF TRANSVERSE SECTION OF Ni-32 w/o Mo
-5.5 w/o Al-1 w/o Ta-3 w/o Cr-0.066 w/o C



EFFECT OF ALUMINUM CONTENT ON RUPTURE LIFE AT 1900°F, 30 KSI OF α -Mo REINFORCED Ni-Al-Mo TERNARY ALLOYS (R = 3 CM/HR, G_L 300°C/CM)



EFFECT OF CHROMIUM CONTENT ON RUPTURE LIFE (1900°F, 30 ksi)
 OF γ'/γ -a ALLOYS CONTAINING 5.5 w/o Al



BREAKUP OF α -Mo RODS CONTAINING VARYING AMOUNTS OF Cr AT 1900 °F AND 30 KSI

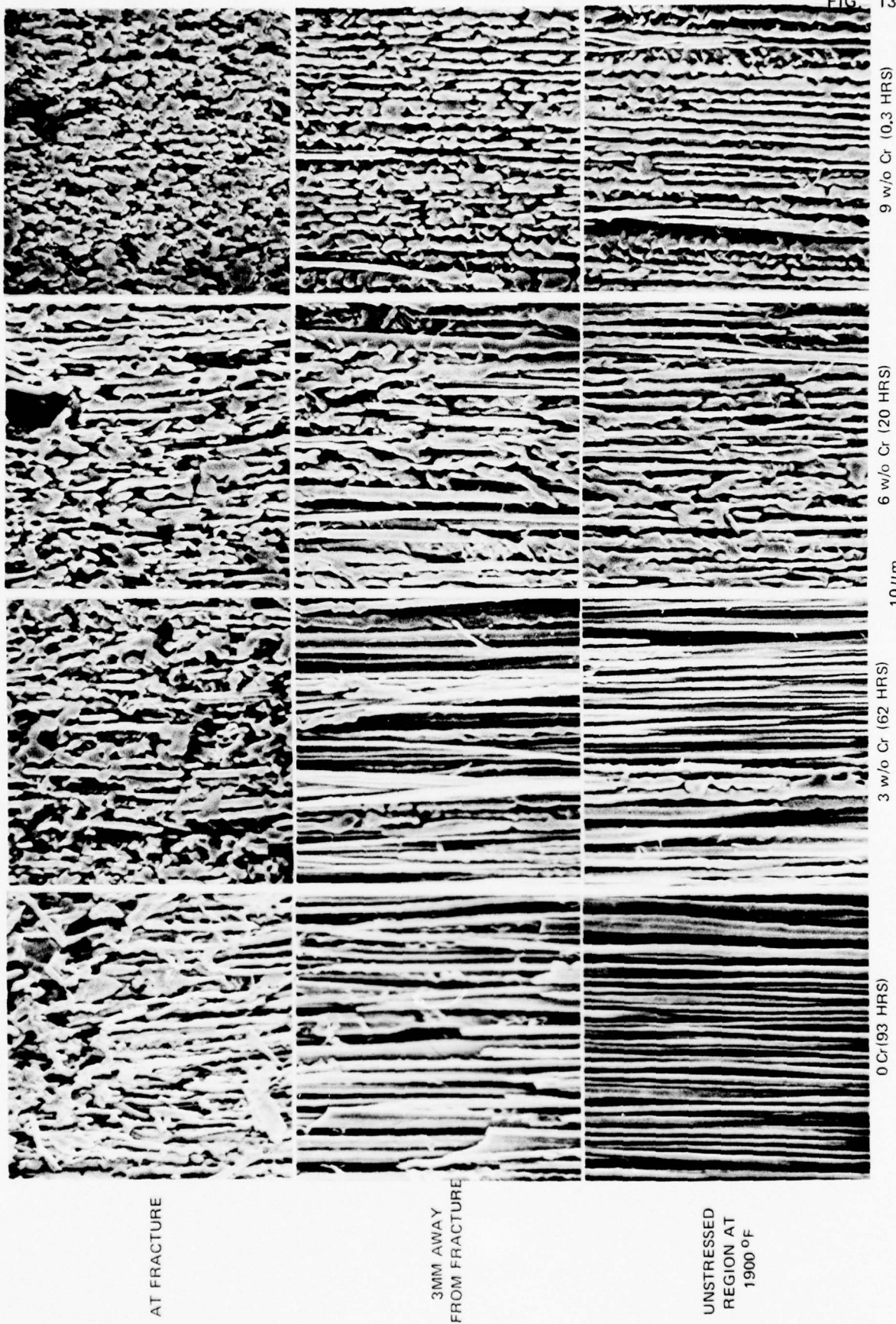


FIG. 13

AT FRACTURE

3MM AWAY
FROM FRACTURE

UNSTRESSED
REGION AT
1900 °F

0 Cr (93 HRS)

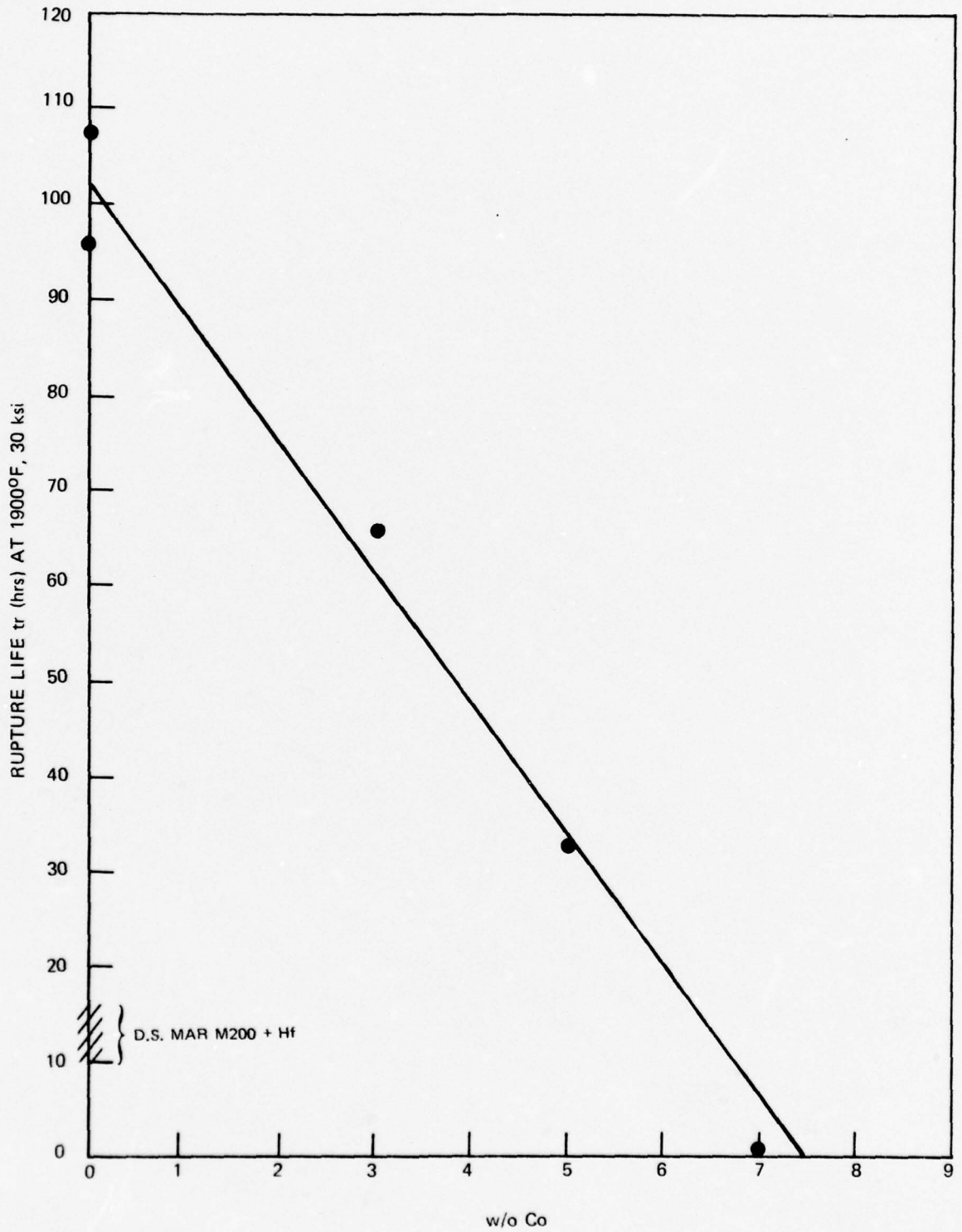
3 w/o Cr (62 HRS)

6 w/o Cr (20 HRS)

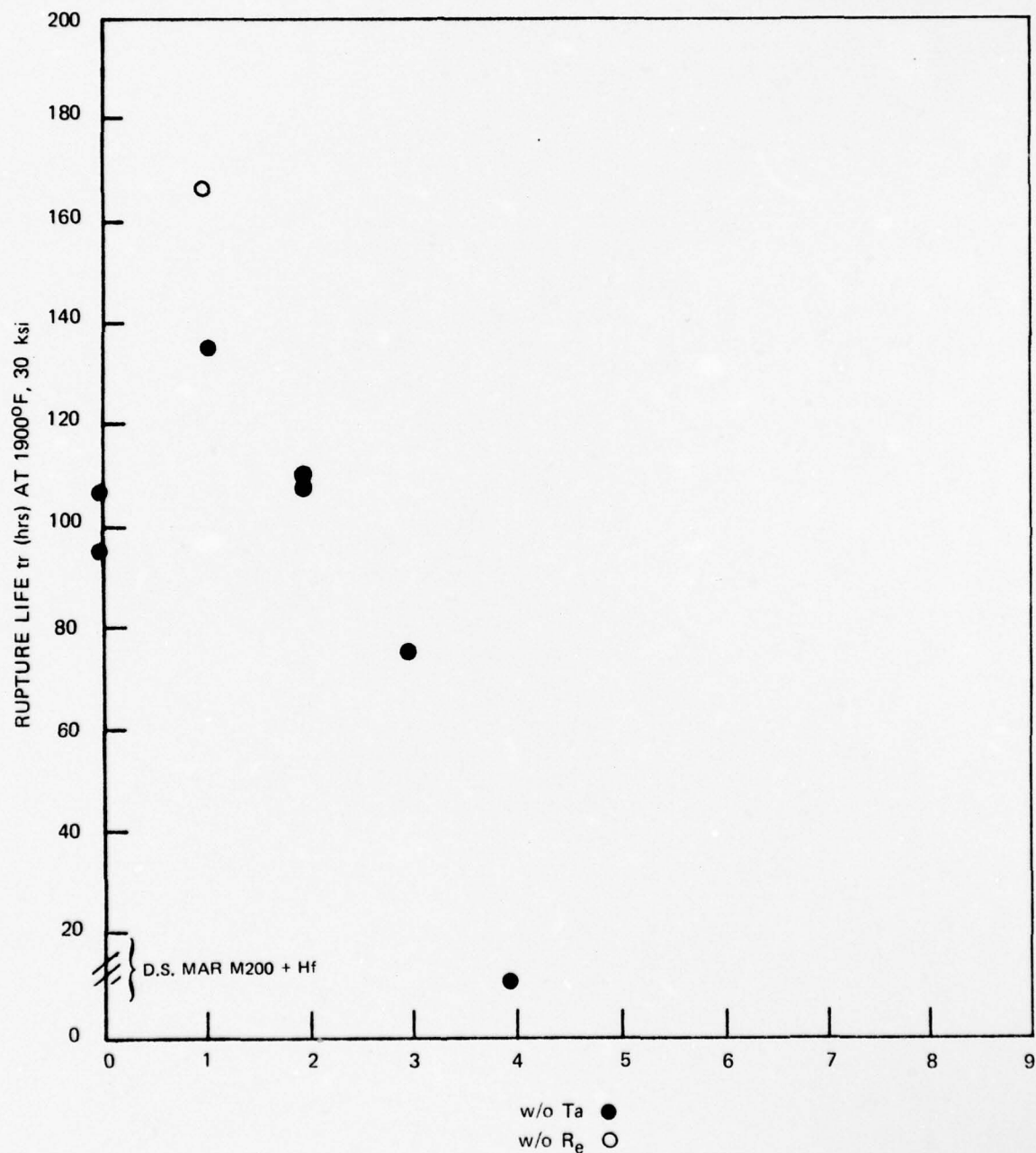
9 w/o Cr (0.3 HRS)

10 μ m

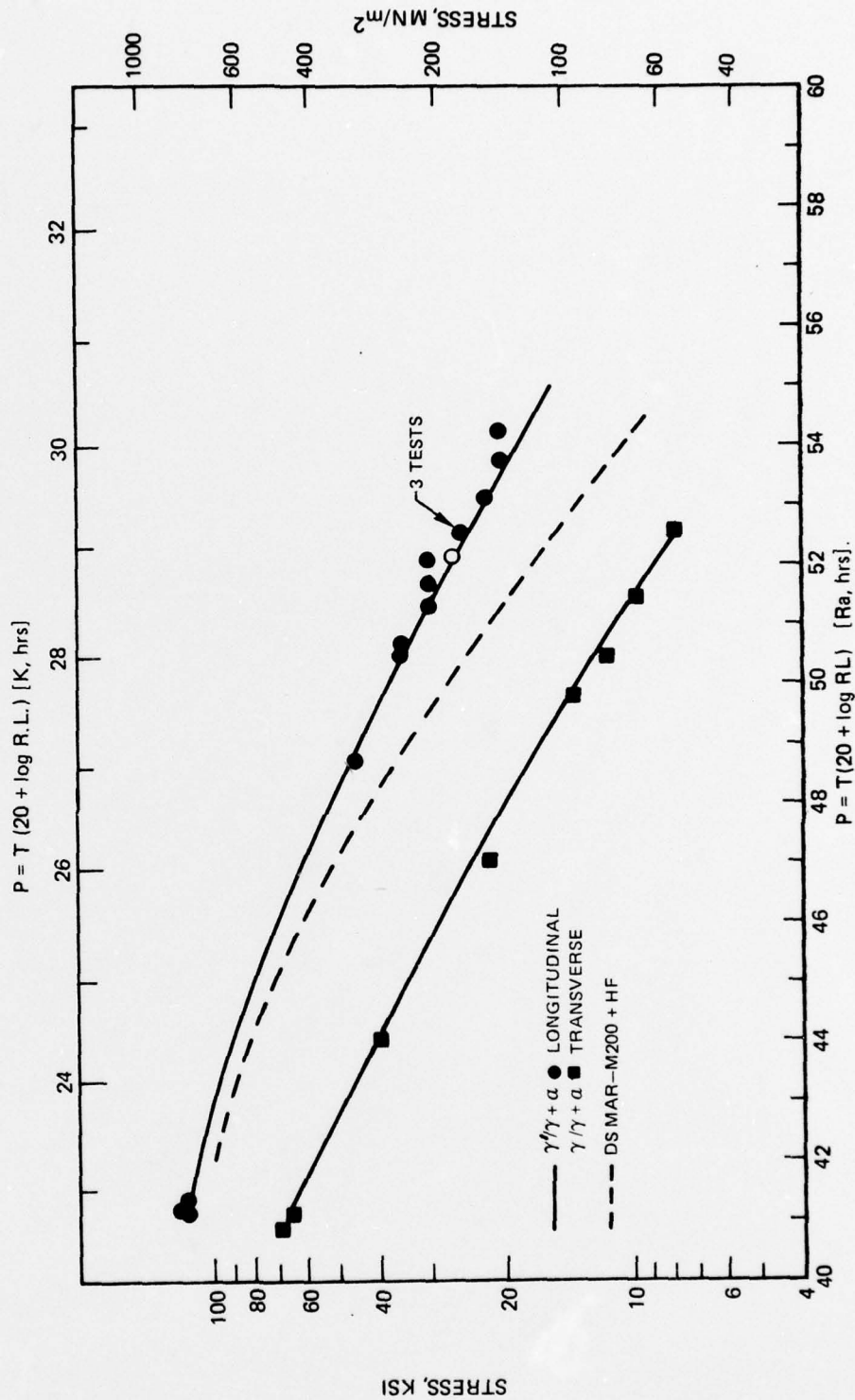
EFFECT OF COBALT CONTENT ON RUPTURE LIFE (1900°F, 30 ksi)
OF γ'/γ -a ALLOYS CONTAINING 5.5 w/o Al



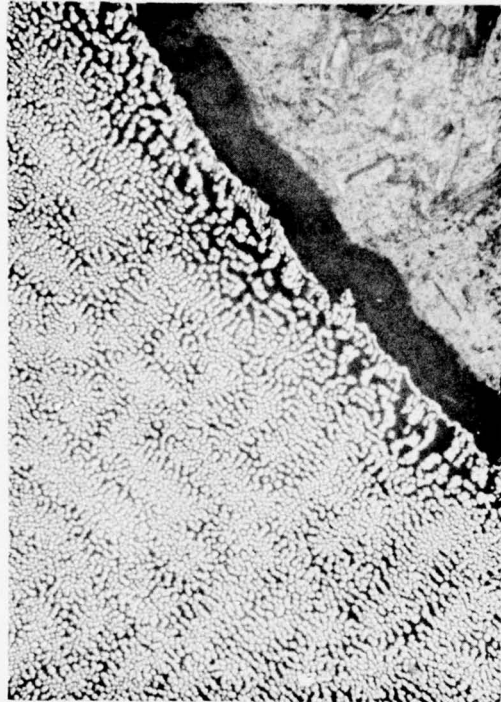
EFFECT OF TANTALUM AND RHENIUM CONTENT ON RUPTURE LIFE (1900°F, 30 ksi)
OF γ'/γ -a ALLOYS CONTAINING 5.5 w/o Al



LARSON MILLER PARAMETER—RUPTURE CURVES OF $\gamma/\gamma-\alpha$ AND D.S. MAR—M200 + HF

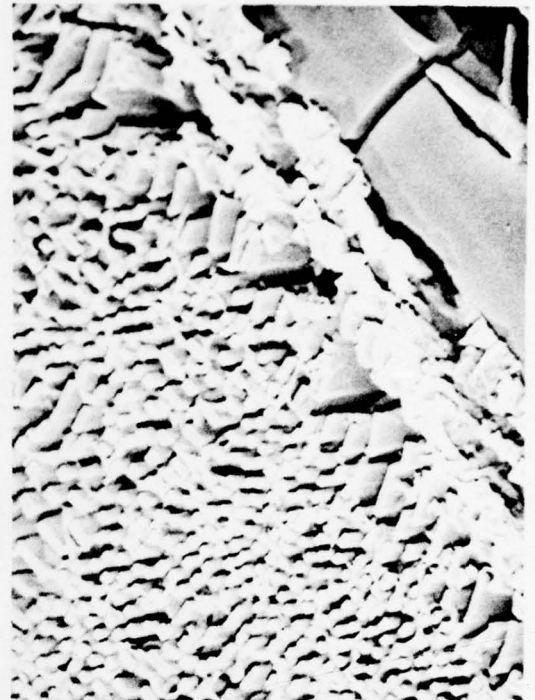


LONGITUDINAL STRESS RUPTURE FRACTURE SURFACES OF TRANSVERSELY ORIENTED Ni-31.5 w/o Mo-6.2 w/o Al



1400°F

50μ



1400°F

5μ

(E591-1)



2000°F

50μ

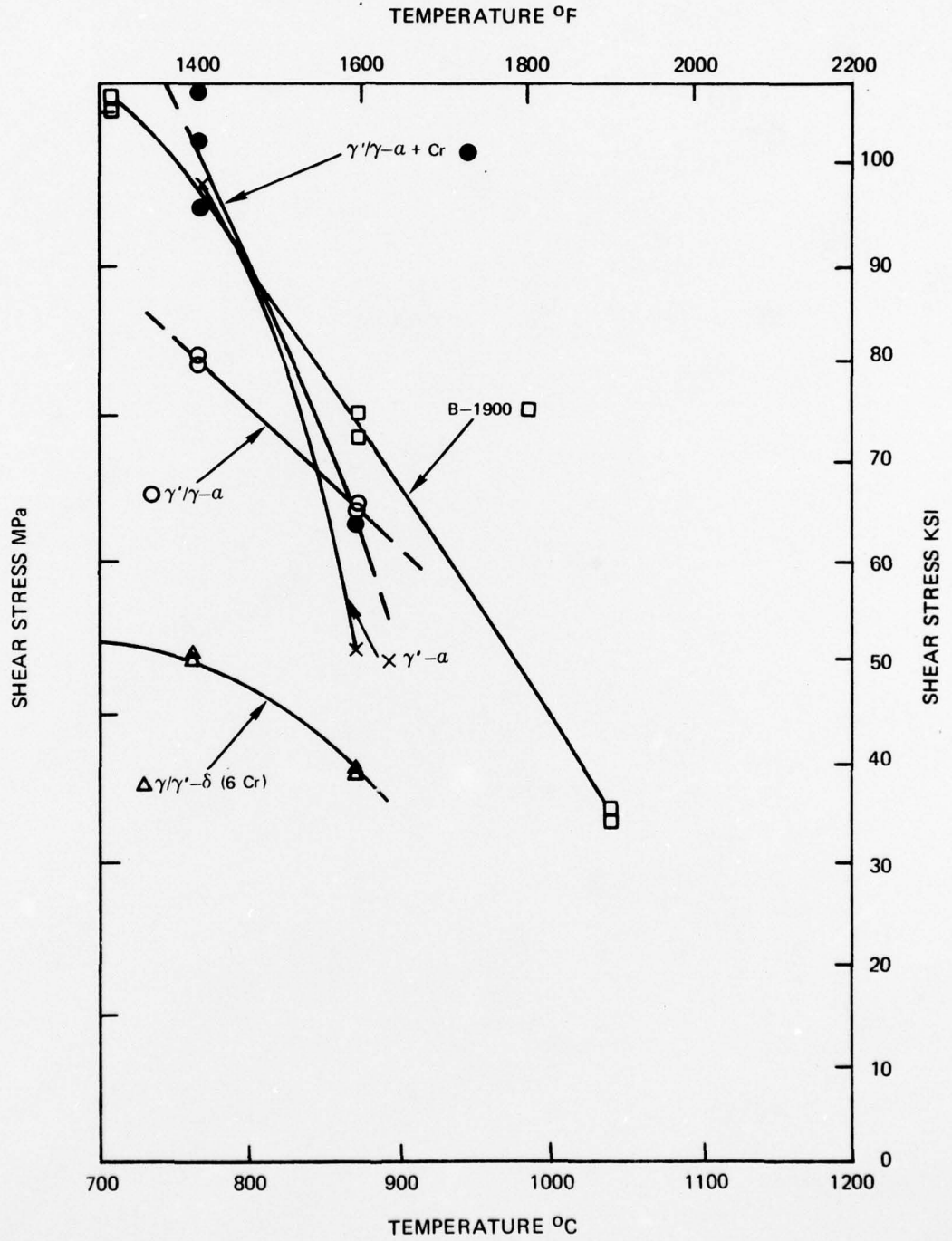


2000°F

5μ

E591-8

ULTIMATE SHEAR STRENGTHS OF D.S. $\gamma'/\gamma-a$ COMPARED WITH
B-1900 AND D.S. $\gamma/\gamma'-\delta$ (6 Cr)



SPECIMEN EXPANSION DURING THERMAL FATIGUE UNDER 10 KSI STRESS (2 MINUTE CYCLES: 750°F-2050°F)

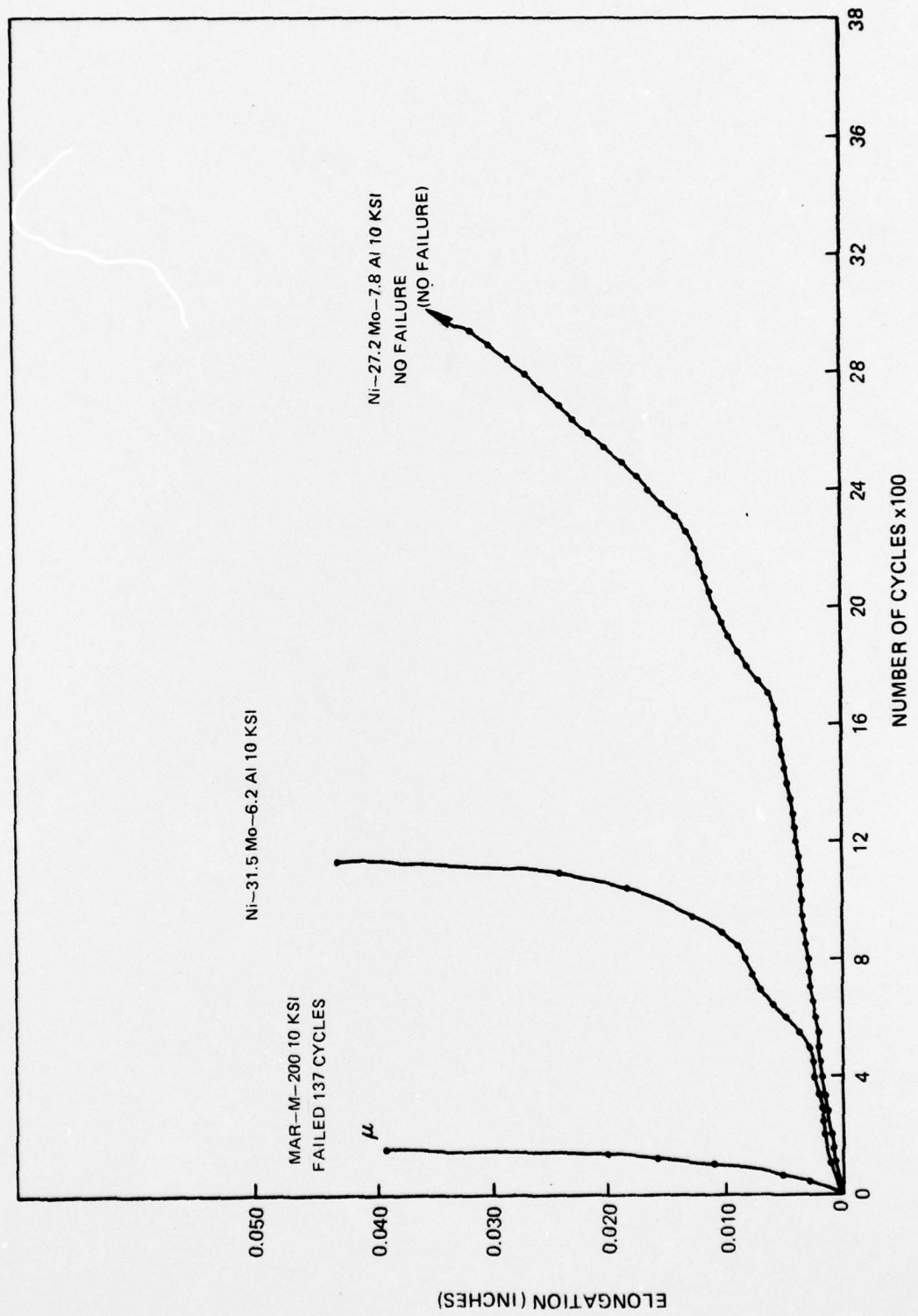
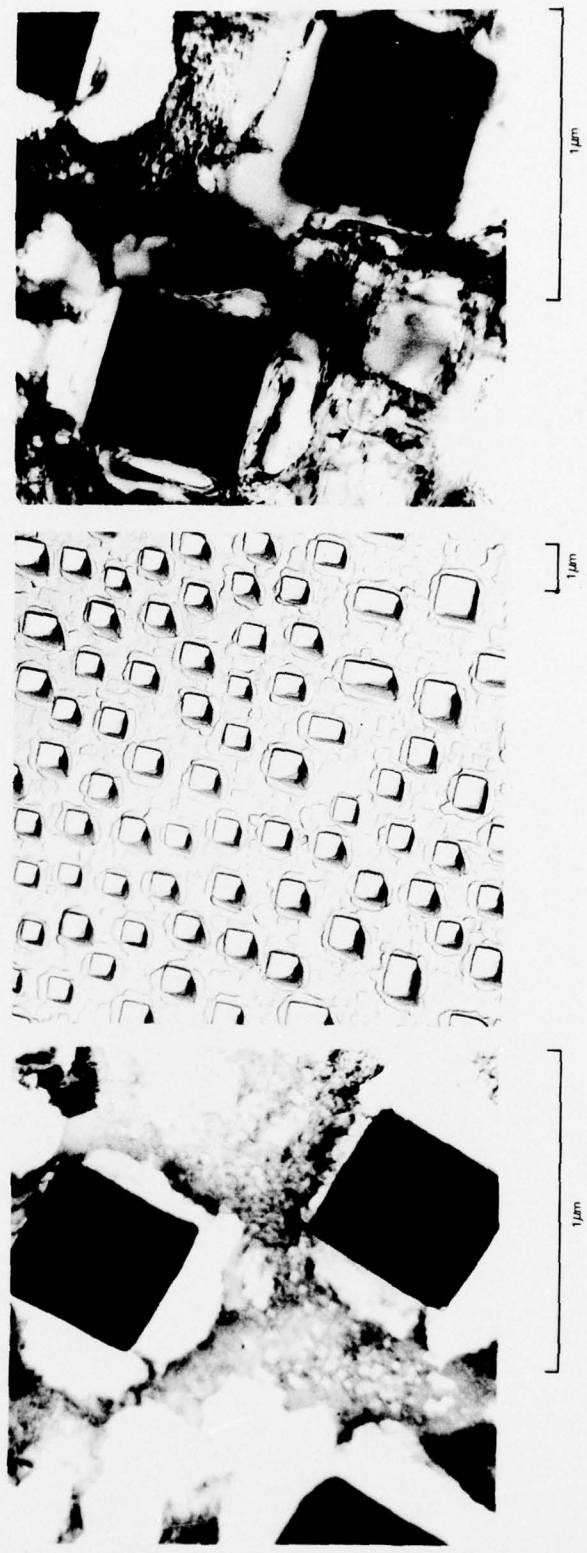


FIG. 19

EFFECT OF 1000 HR EXPOSURE AT 1100°C (2012°F) ON THE MICROSTRUCTURE OF γ/γ' -Al (Ni-37.5 w/o Mo-47 w/o Al)



a) AS DIRECTIONALLY SOLIDIFIED
b) POST EXPOSURE
c) POST EXPOSURE

FIG. 21

THERMAL EXPANSION OF $\gamma/\gamma-\alpha$ (Ni-31.5 w/o Mo-6.2 w/o Al)

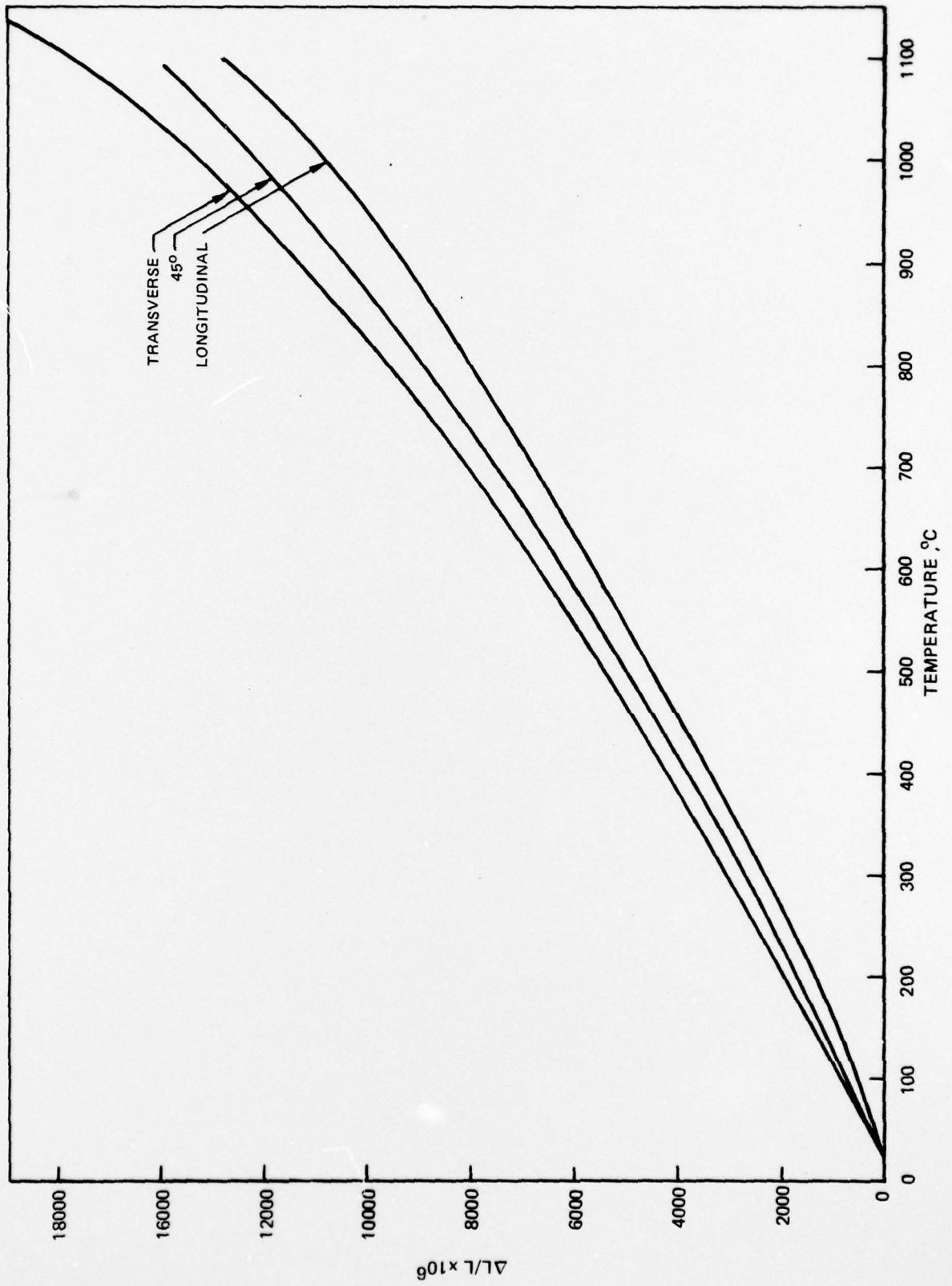
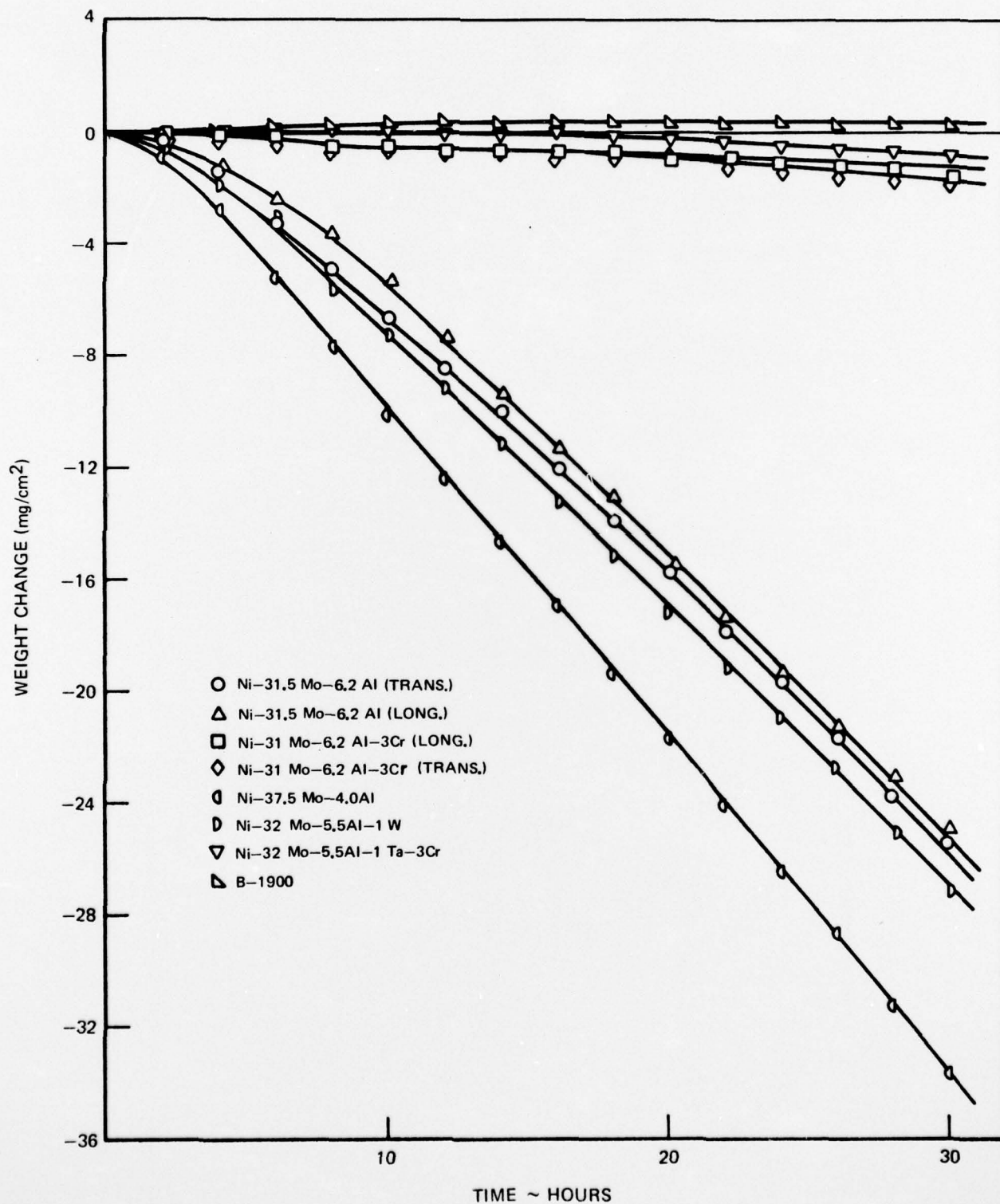


FIG. 22

CYCLIC OXIDATION OF MODIFIED γ'/γ - α ALLOYS IN AIR AT 1000° C



DISTRIBUTION LIST

(One copy unless otherwise noted)

(3 copies plus balance after distribution)

U. S. Naval Air Systems Command
(AIR-52031B)
Department of the Navy
Washington, DC 20361

(7 copies, for internal distribution by AIR-954, as follows:)

AIR-954 (2 copies), AIR-536B1 (1 copy); AIR-330A (1 copy), AIR-330B
(1 copy), AIR-5361A (1 copy), AIR-5362A (1 copy)
U. S. Naval Air Systems Command
(AIR-6043 (5 copies)
Department of the Navy
Washington, DC 20361

(2 copies)

Commander, Naval Air Development Center
Code 302A, A. Fletcher (1 copy)
Code 30232, E. Tankins (1 copy)
Warminster, PA 18974

U. S. Naval Air Turbine Test Station (2 copies)
Attn: J. Glatz (PE-43) (1 copy), A. Martino (AT-1) (1 copy)
1440 Parkway Avenue
Trenton, NJ 08628

U. S. Naval Sea Systems Command (Code 035)
Department of the Navy
Washington, DC 20362

Commander, Naval Weapons Center
Code 5516
China Lake, CA 93555

U. S. Naval Ships Engineering Center (Code 6146)
Department of the Navy
Center Building
Prince George's Center
Hyattsville, MD 20782

Naval Weapons Laboratory
Attn: W. Mannschreck
Dahlgren, VA 22448

U. S. Naval Ships Research and Development Center
Code 2812
Annapolis, MD 21402

DISTRIBUTION LIST

Naval Surface Weapons Center (Metallurgy Division)
White Oak
Silver Spring, MD 20910

(2 copies)

Director, Naval Research Laboratory
(Code 6300 (1 copy))
(Code 6350 (1 copy))
Washington, DC 20390

Office of Naval Research
The Metallurgy Program, Code 471
Arlington, VA 22217

(2 copies)

Director, Army Materials and Mechanics Research Center
(A. Gorum - 1 copy) (P. Ahearn - 1 copy)
Watertown, MA 02172

U. S. Army Aviation Materiel Laboratories
Fort Eustis, VA 23604

Commander, U. S. Army Munitions Command
Frankford Arsenal
(Attn: D. Kleppinger)
Pitman Dunn Laboratory
Philadelphia, PA 19137

(4 copies)

Air Force Materials Laboratory
Code AFML/LLM (Capt. R. M. Dunco) (1 copy)
Code LLS (1 copy)
Code AFML/MXE (Mr. A. Olevitch) (1 copy)
Code AFML/MXE (1 copy)
Wright-Patterson Air Force Base, OH 45433

Air Force Aero Propulsion Laboratories
Attn: Capt. D. Zabierek, Code TBP
Wright-Patterson Air Force Base, OH 45433

National Aeronautics & Space Administration
Code RWM
Washington, DC 20546

DISTRIBUTION LIST

Robert L. Parker
Crystallization of Metals Section
National Bureau of Standards
Bl64 Materials Building
Washington, DC 20234

(3 copies)
National Aeronautics & Space Administration
Lewis Research Center
(G. M. Ault - (1 copy))
(H. P. Probst - (1 copy))
(C. Scheuermann - (1 copy))
21000 Brookpark Road
Cleveland, OH 44135

U. S. Energy Research and Development Administration
Division of Reactor Research and Development
(A. Van Echo)
Washington, DC 20545

Metals and Ceramics Information Center
Battelle Columbus Laboratories
505 King Avenue
Columbus, OH 43201

The John Hopkins University
Applied Physics Laboratory
(Maynard L. Hill)
8621 Georgia Avenue
Silver Spring, MD 20910

AVCO RAD
201 Lowell Street
Wilmington, MA 01887

IIT Research Institute
(Dr. N. Parikh)
10 West 35th Street
Chicago, IL 60616

Detroit Diesel Allison Division
General Motors Corporation
Materials Laboratories
Indianapolis, IN 46206

DISTRIBUTION LIST

Pratt and Whitney Aircraft Division
United Technologies Corporation
East Hartford, CT 06108

Clevite Company Mechanical Research Division
Attn: Mr. A. D. Schwope
540 East 105th Street
Cleveland, OH 44108

Lycoming Division
AVCO Corporation
Stratford, CT 06497

Curtis-Wright Company
Wright Aeronautical Division
Wood-Ridge, NJ 07075

Bell Aerosystems Co.
Technical Library
P.O. Box 1
Buffalo, NY 14240

General Electric Co.
Aircraft Engine Group
Materials & Processes Technology Labs
Ewendale, OH 45215

Solar
Dr. A. Metcalfe
2200 Pacific Highway
San Diego, CA 92112

Teledyne CAE
1330 Laskey Road
Toledo, OH 43601

Stellite Div.
Cabot Co.
Technical Library
P.O. Box 746
Kokomo, IN 46901

Materials Research Co.
Attn: Dr. S. Weinig
Orangeburg, NY 10962

DISTRIBUTION LIST

Artech Co.
Attn: Mr. Henry Hahn
2816 Fallfax Drive
Falls Church, VA 22042

Dr. Merton C. Flemings
Room 35-316
MIT
Cambridge, MA 02139

Prof. R. W. Kraft
Dept. of Met. & Materials Science
Lehigh Univ.
Bethlehem, PA 18015

Prof. N. J. Grant
Dept. of Met. & Materials Science
MIT
Cambridge, MA 02139

Dr. Kenneth A. Jackson
Bell Telephone Laboratories, Inc.
600 Mountain Ave.
Murray Hill, NJ 07974

National Academy of Sciences
Materials Advisory Board
Attn: Dr. J. Lane
Washington, DC 20418

Reynolds Metal Co.
Attn: Technical Library
Reynolds Metals Bldg.
Richmond, VA 23218

P. R. Mallory & Co. Inc.
Attn: Technical Librarian
3029 East Washington St.
Indianapolis, IN 46206

Midwest Research Institute
425 Valken Boulevard
Kansas City, MO 64110

DISTRIBUTION LIST

Aluminum Co. of America
Attn: Mr. G. B. Barthold
1200 Ring Bldg.
Washington, DC 20036

Prof. Alan Lawley
Head, Dept. of Met. Eng.
Drexel Univ.
32nd & Chestnut Sts.
Philadelphia, PA 19104

Dr. A. I. Mlavsky
Tyro Laboratories, Inc.
16 Hickory Drive
Waltham, MA 02145

Whittaker Co.
Nuclear Metals Div.
Attn: Dr. A. S. Bufford
West Concord, MA 01781

University of California
Lawrence Radiation Laboratory
Attn: Technical Information Div.
Livermore, CA 94550

TRW Equipment Laboratories
Attn: Mr. J. A. Alexander
23555 Euclid Avenue
Cleveland, OH 44117

General Electric Co.
Corporate Research & Development
Mr. G. Benz
P.O. Box 8
Schenectady, NY 12301

General Electric Co.
Corporate Research & Development
Dr. James D. Livingston
P.O. Box 8
Schenectady, NY 12301

DISTRIBUTION LIST

Westinghouse Electric Co.
Materials & Processing Labs
Attn: R. Begley
Beulah Road
Pittsburgh, PA 15235

Final Report Only (12 copies)
Commander, Naval Air Development Center
Code 302A, A. Fletcher - For DDC
Warminster, PA 18974

Final Report Only (3 copies)
Commander, Naval Air Development Center
Code 813
Warminster, PA 18974